



e.3

# NATIONAL ADVISORY COMMITTEE FOR AERONAUTICS

TECHNICAL MEMORANDUM

No. 1202

ON WIND TUNNEL TESTS AND COMPUTATIONS CONCERNING  
THE PROBLEM OF SHROUDED PROPELLERS

By W. Krüger

Translation of ZWB Forschungsbericht Nr. 1949, January 21, 1944



Washington  
February 1949

NATIONAL ADVISORY COMMITTEE FOR AERONAUTICS

TECHNICAL MEMORANDUM NO. 1202

ON WIND TUNNEL TESTS AND COMPUTATIONS CONCERNING  
THE PROBLEM OF SHROUDED PROPELLERS\*

By W. Krüger

**Abstract:** Results of measurements on a shrouded propeller are given. The propeller is designed for high ratio of advance and high thrust loading. The effect of the shape of propeller and shroud upon the aerodynamic coefficients of the propulsion unit can be seen from the results. The highest efficiency measured is 0.71. The measurements permit the conclusion that the maximum efficiency can be essentially improved by shroud profiles of small chord and thickness. The largest static thrust factor of merit measured reaches, according to Bendemann, a value of about  $\xi = 1.1$ . By the use of a nose split flap the static thrust for thin shroud profiles with small nose radius can be about doubled. In a separate section numerical investigations of the behavior of shrouded propellers for the ideal case and for the case with energy losses are carried out. The calculations are based on the assumption that the slipstream cross section depends solely on the shape of the shroud and not on the propeller loading. The reliability of this hypothesis is confirmed experimentally and by flow photographs for a shroud with small circulation. Calculation and test are also in good agreement concerning efficiency and static thrust factor of merit. The prospects of applicability for shrouded propellers and their essential advantages are discussed.

**Outline:**

- A. Introduction
- B. Symbols and Definitions
- C. Model Specifications and Test Procedure
- D. Test Results

---

\*"Windkanalmessungen und Rechnungen zum Problem der ummantelten Luftschraube." Zentrale für wissenschaftliches Berichtswesen der Luftfahrtforschung des Generalluftzeugmeisters (ZWB) Berlin-Adlershof, Forschungsbericht Nr. 1949, Jan. 21, 1944.

## E. Theoretical Considerations

### I. Propeller in forward motion

### II. Propeller at rest

## F. Additional Measurements Concerning the Problem of the Slipstream Cross Section and of the Pressure Losses for Flow through the Shroud

## G. Comparison between Calculation and Measurement

## H. Summary and Conclusions

## K. References

### A. INTRODUCTION

The power limits of the production of propulsion by means of propellers as they are in use today have been discussed repeatedly elsewhere. The larger the velocity region to be covered, the harder it is to reach the ideal goal: to transform with one and the same propeller the expended power with the best efficiency into useful power for both limiting operating conditions, static and high speed as well as for all intermediate states. For present flight velocities one must depend for the design of the propellers on a compromise solution which is necessarily bound to bring about considerable losses of propulsion power for certain operating conditions. The limits of the obtainable static thrust were treated in detail by A. Bez [1]<sup>1</sup>. According to him, the propeller diameters, in order to obtain a sufficient static thrust, usually have to be larger than would be necessary for high speed. The efficiencies in flight then do not reach their possible optimum values. Measurements on shrouded propellers have demonstrated that with arrangements of this kind very considerable improvements of static thrust can be obtained. The use of a shroud is, therefore, a means to extend the power limits of the normal propeller. An added advantage of the shroud can be found in the fact that due to the additional velocities in the propeller plane due to the shroud, the propeller itself will experience smaller changes in operating condition for a change of the advance ratio than will a normal propeller. This means a possible reduction in the range of blade angle change, perhaps even permitting the application of fixed pitch propeller blades. Since the propeller diameter may be reduced because of the better static thrust factor of merit the propellers may, circumstances permitting, be run at the motor rpm and thus avoid the use of a gear system. If the occasion arises one could sometimes proceed to increase further the motor rpm.

---

<sup>1</sup>Translator's Note: Numbers in brackets refer to the references at the end of the report.

The nozzle propeller has been used for a long time very successfully in shipbuilding as Kort nozzle. Its application in airplane construction is rendered more difficult particularly by the fact that the intrinsic drag of the shroud is, in view of the essentially smaller thrust loading coefficient of the airplane propeller at high forward speed, of much greater importance than for the ship propeller at the fastest forward motion. The problem was repeatedly taken up because of the great possibilities of improvement for static conditions and because of the possibility of reducing the Mach number at the blade tip by a suitable shape of the shroud. Recent results can be found in the publications by B. Regenscheit [2], D. Küchemann and J. Weber [3], and M. Hansen [4].

The behavior of shrouded propellers was also repeatedly investigated theoretically. W. Stiess [5] extended the momentum theory to nozzle propellers with and without guide vanes. Furthermore, a treatise by O. Pabst [6] deals with the calculation of shrouded propellers. Then the problem was treated very thoroughly by D. Küchemann and J. Weber [3] by application of potential theoretical considerations to annular profiles.

The tests carried out so far resulted in a valuable preliminary clarification of the problems of interest. However, many single problems could not be solved because the model arrangements which were used did not permit a separate treatment of the effect of various configurations upon propeller and shroud. Moreover, investigations of shrouded propellers were desirable which about corresponded to today's requirements for high power airplanes regarding their region of advance ratio, thrust loading and power loading.

The firm Dornier-Werke G.m.b.H. showed great interest in these measurements in particular, in view of the application as pusher propeller. The shrouded propeller appears especially suited for this case, because it requires small diameters. Furthermore, it is absolutely possible to use the shroud simultaneously as damping surface so that the doubts mentioned above are of no importance because of the intrinsic drag of the shroud.

The present report gives the test results on a shrouded propeller which was designed according to the present knowledge for a high ratio of advance and relatively high thrust loading. The forces at the propeller and at the shroud were measured separately. The detailed investigations also permit the inclusion of the influence of energy losses upon the aerodynamic behavior of the shrouded propeller and therewith a clear representation of the theory of the shrouded propeller subject to losses. In particular the test results make it possible to elucidate the

behavior for static conditions and to estimate the attainable limits of static thrust for shrouded propellers.

Due to the separate suspension of nacelle and shroud the supporting elements of the shroud which were necessary in full scale could be omitted for the model. However, this deviation of the model test from full scale conditions is not very important because it will be useful to develop the supporting struts also on the full scale model as guide vanes.

## B. SYMBOLS AND DEFINITIONS

### Subscripts:

S	propeller
M	shroud
Go	nacelle
N	nose split ring
Pr	profile
R	annular area between shroud and nacelle
o	condition without propeller
th	theoretical
$\infty$	condition far behind the propeller

### Lengths:

x	coordinate in the direction of the axis
$l_{Go}$	length of the nacelle
l	chord of the shroud, measured parallel to the axis
$l_{Pr}$	shroud chord, measured in the direction of the chord of the shroud profile
D	diameter of the propeller
R	radius of the propeller

$D_{hub}$	diameter of the hub in the propeller plane
$u$	hub ratio $D_{hub}/D$
$D_{Go}$	diameter of the nacelle
$D_M$	mean shroud diameter
$D_N$	maximum diameter of the nose split ring
$d$	maximum profile thickness of the profile of the shroud and of the propeller blade, respectively
Angles:	
$\beta$	angle of adjustment of the outer propeller blade profile measured between chord and plane of rotation
$\delta$	inclination of the line bisecting the trailing-edge angle of the shroud profile toward the axis
Areas:	
$F = \frac{D^2\pi}{4}$	propeller disk area
$F_{\infty}$	cross section of the slipstream at infinite distance behind the propeller
$\alpha$	ratio of the slipstream cross section $\frac{F_{\infty}}{F}$
$F^*$	chord area of the shroud $D_M \pi l_{Pr}$
$F_A$	free exit cross section in the trailing edge plane of the shroud
$F_R$	annular area between shroud and nacelle
$F_{RS} = F(1 - u^2)$	annular area between shroud and nacelle, measured at disc plane
$F_{Rmin}$	minimum annular cross section between nacelle and shroud

Velocities and significant ratios:

\* index for the velocities for static condition

$v$	free stream velocity
$q = \frac{\rho}{2} v^2$	stagnation pressure of the free stream
$u$	maximum circumferential velocity of the propeller
$\lambda$	ratio of advance $v/u$
$w_a$	axial additional velocity in the slipstream at infinity behind the propeller
$Q(\text{m}^3/\text{s})$	quantity of air flowing through the annular shroud cross section
$\bar{v}_R = \frac{Q}{F_R}$	mean axial flow velocity through the annular area between nacelle and shroud
$\bar{v}_{R\text{max}} = \frac{Q}{F_{R\text{min}}}$	mean axial flow velocity through the minimum annular area $F_{R\text{min}}$ between shroud and nacelle
$\bar{v}_{RS} = \frac{Q}{F_{RS}}$	mean axial flow velocity through the annular area between nacelle and shroud, measured in the rotation plane of the propeller
$\phi = \frac{\bar{v}_{RS}}{u}$	mass coefficient - inner advance ratio
$v_r$	local axial flow velocity through the annular area, measured for the radius $r$
$v_\infty$	axial velocity in the slipstream infinitely far behind the propeller
$\delta_o$	dimensionless additional velocity $\frac{\bar{v}_{RS} - v}{v}$ for the condition without propeller, due only to shroud circulation
$\delta_{o\text{th}}$	theoretical value of the dimensionless additional velocity for the condition without propeller, due only to shroud circulation
$\delta_S$	dimensionless additional velocity in the rotation plane of the propeller caused by the additional circulation of the shroud due to propeller loading
$\delta_g$	dimensionless total additional velocity $\frac{\bar{v}_{RS} - v}{v}$ due to the shroud circulation and the propeller loading

## Propeller and shroud coefficients:

\* index for coefficients for static conditions

$$k_{SS} = \frac{S_s}{\frac{\rho}{2} u^2 F}; \quad c_{SS} = \frac{S_s}{\frac{\rho}{2} v^2 F}$$

coefficients of the propeller thrust

$$k_{SM} = \frac{S_M}{\frac{\rho}{2} u^2 F}; \quad c_{SM} = \frac{S_M}{\frac{\rho}{2} v^2 F}$$

coefficients of the shroud thrust

$$\bar{k}_s = \frac{\bar{S}}{\frac{\rho}{2} u^2 F}; \quad \bar{c}_s = \frac{\bar{S}}{\frac{\rho}{2} v^2 F}$$

coefficients of the total thrust of the shrouded propeller not subject to losses

$$\bar{k}_{se} = \frac{\bar{S}_e}{\frac{\rho}{2} u^2 F}; \quad \bar{c}_{se} = \frac{\bar{S}_e}{\frac{\rho}{2} v^2 F}$$

effective total thrust coefficient of the shrouded propeller subject to losses

$$\bar{c}_{s1} = \bar{c}_{se} + c_{wM} + \Delta c_w$$

loading ratio (definition)

$$k_l = \frac{L}{\frac{\rho}{2} u^3 F}$$

power coefficient

$L_1$  according to definition: power which is put into the propeller shaft

$$\eta = \frac{\bar{k}_s}{k_l} \lambda$$

propulsion efficiency

$\eta_m$  maximum theoretical efficiency

$\eta_{Ma}$  efficiency of the shroud

$\eta_E$  efficiency of configuration

$\eta_G$  blower efficiency or factor of merit of the propeller

$$\zeta = \frac{\bar{k}_s^*}{(2k_l^*)^{2/3}}$$

static thrust factor of merit according to Bendemann

$$\zeta_U = \frac{\bar{k}_S^*}{2\alpha^{*1/3} k_T^{*2/3}} \quad \text{static thrust factor of merit of the shrouded propeller}$$

$$\psi = \frac{\Delta p_g}{\frac{\rho}{2} u^2} \quad \text{pressure coefficient of the blower}$$

$$\sigma = \frac{\phi^2}{\psi} = \frac{\frac{\rho}{2} v_{RS}^2}{\Delta p_g} \quad \text{characteristic value for the operating condition of the blower}$$

$$c_{nPr} \quad \text{normal force coefficient of the shroud profile} \\ \text{(The normal force is, according to definition, positive if directed toward the axis.)}$$

Drag and loss coefficients:

$$\Delta p_v \quad \text{total pressure loss}$$

$$\Delta p_g \quad \text{total pressure jump of propeller and stator}$$

$$c_w = \frac{W}{q \times F} \quad \text{actual parasite drag coefficient referred to} \\ F = D^2 \pi / 4$$

$$c_w^* = \frac{W}{q \times F^*} \quad \text{actual parasite drag coefficient referred to} \\ F^* = D_M \pi l_{Pr}$$

$$c_w^i \quad \text{drag coefficient measured including induction}$$

$$\Delta c_{wGO1} \quad \text{drag induced by the shroud on nacelle}$$

$$\Delta c_{wM1} \quad \text{drag induced by the nacelle on shroud}$$

$$\Delta c_w \quad \text{additional drag caused by the increased relative} \\ \text{velocity at nacelle and shroud due to propeller} \\ \text{loading}$$

$$\eta_D \quad \text{efficiency of the diffuser}$$

$$\mu = \frac{\Delta p_v}{\frac{\rho}{2} v^2} \quad \text{energy loss referred to the stagnation pressure} \\ \text{of the free-stream velocity which occurs for} \\ \text{flux through the shroud due to friction and} \\ \text{separation on the surface of the shroud and} \\ \text{the nacelle}$$

$$\mu_e = \frac{\Delta p_v}{\frac{\rho}{2} \overline{v_R}^2}$$

energy loss in the flow through the shroud referred to the stagnation pressure at smallest cross section of annular shroud area

C. MODEL SPECIFICATIONS AND TEST PROCEDURE

The model of the shrouded propeller under investigation is reproduced in figure 1 and in the photographs 2 to 4.

The body of the nacelle has the shape of an ellipsoid; it was calculated so that smallest possible additional velocities will occur in the flow about it. In the nacelle body there is a high speed a.c. motor (type AVA - SDM - E) which, for rpm of 30,000 has a maximum output of 30 PS (German hp).

The adjustable 8-blade propeller was supported by roller bearing on the shaft of the motor. It has a diameter of 240 millimeters and a hub ratio  $D_{hub}/D = 0.35$ . The propeller was calculated by a method which is customary for the design of axial blowers. The design was based on the following criteria: outer advance ratio  $\lambda = \frac{v}{u} = 0.95$  and the total thrust loading of the propeller including the shroud  $\bar{c}_s = \frac{\bar{S}}{\frac{\rho}{2} v^2 F} = 0.15$ . For full scale these

relations will approximately hold true if an effective total thrust of  $\bar{S}_e = 400$  kg is to be reached for a flight velocity of 800 km/h at a height of 8.6 km for a tip velocity of 230 m/s by means of a propeller of 1.65 m  $\phi$ . The number of revolutions for this case would be 2700/min, that is, the same as the motor rpm in use today. Therefore the gear system could be omitted. The effective propulsion power would be  $L_e = \bar{S}_e \times v = 1185$  PS (German hp). In order to design the propeller one must know the mean axial flow velocity  $\overline{v_{RS}}$  through the propeller disc area, that is, the inner ratio of advance  $\phi = \frac{\overline{v_{RS}}}{u}$  and also the distribution of the total thrust on propeller and shroud. These two values which are a priori unknown are functions of the shape of the shroud and the total thrust loading. For the first design they were estimated according to earlier theoretical investigations and measurements on shrouded propellers [3]. The additional condition had to be taken into consideration that due to the effect of the shroud the inner ratio of advance ( $\phi$ ) has to be lower by 20 percent than the outer one ( $\lambda$ ) according to design (high speed) in order to reduce the Mach number. After the approximate mass and pressure coefficient

of the blower had been determined from these calculations, the necessary construction specifications (number of blades, shape of the blade, angle of incidence) could be calculated so as to obtain a good blower efficiency for this condition.

Two propellers were investigated in this test which differed only with respect to the pitch distribution. Since the distribution of the axial flow velocity along the radius of the propeller was not known for propeller number 1 as a first approximation the axial velocity was assumed to be independent of  $r$ . The calculation yielded, under the condition of design that the wing circulation along the radius should remain the same, the dimensions of the propeller blade shown in figure 5. The NACA series 23009 - 23012 was used for the profiles and was adjusted to the cascade flow by giving the chord larger camber (approximation method according to [7]). The angle of blade setting for the propeller number 2 is increased on the outside as compared with propeller number 1, in order to allow in the test for the probable increase of the axial flow velocity toward the outside and for the effect of this increase upon the efficiency. The propeller profiles can be taken from figure 6.

The investigations were carried out partly with, partly without stator vanes. For reasons of construction and measuring technique the stator vanes in the model had to be fixed behind the propeller and attached to the shroud on the outside. Its characteristic values may be taken from figure 5.

The propeller was examined in operation with 15 different shrouds. The shroud profiles which were investigated are reproduced in figure 7. The shroud profiles as well as the shape of the body of the nacelle were calculated by D. Küchemann and J. Weber (AVA). The flow variations ( $\delta_{0th}$ ) of the shrouds in a free stream (with nacelle, without propeller) which were theoretically determined can be taken from the table in figure 7. The following dimensions of the shroud profiles were varied: chord, thickness, angle of incidence, and camber.

The following were determined by measurement: thrust of the propeller, thrust of the shroud (separate suspension of nacelle and shroud) and also torque of the propeller for varied propeller pitch and ratio of advance. Furthermore, the drag of the shroud and the nacelle without propeller was measured. The number of revolutions for the propeller could be determined by means of an electric tachometer. The pressure distribution on the nacelle and on the shroud profile was taken with and without propeller in motion, as well as the distribution of the axial flow velocity along the radius immediately ahead of the propeller plane.

These tests were carried out in wind tunnel IV of the AVA (1.25m<sup>2</sup>).

Adjoining the main investigation, several tests were carried out in a small tunnel (Wiss 4: 1.0 x 0.68 meter elliptic) which were to elucidate the problems of jet contraction and expansion for shrouded propellers.

#### D. TEST RESULTS

Neither the Reynolds nor the Mach number could be kept constant for the tests for reasons of power and because of the large range of the ratio of advance. For the maximum case the Reynolds number referred to D was  $Re = 1.2 \times 10^6$  and the Mach number referred to the tip velocity was  $M = 0.45$ .

Only the essential ones out of the numerous arrangements that were measured are reported below. The shrouds designated in figure 7 by 1 and 5c were investigated more thoroughly than the rest of the shrouds in their operation with the propellers 1 and 2, respectively.

1. Nacelle. - Due to mutual influence additional axial forces appear at the nacelle and at the shroud which neutralize each other, that is, the force induced by the shroud at the nacelle  $W_{G01}$  appears in the same magnitude but with inverted sign on the shroud. D. Küchemann and J. Weber [3] already pointed out this fact. All shrouds were investigated with and without nacelle body. Figure 8 shows the dependence of the force induced by the shroud on the nacelle on the dimensionless flow coefficient which was determined for a condition with nacelle. For those shrouds which increase the mass flow the nacelle has an additional drag, for those which decrease it an additional propulsion. From figure 9 one can recognize how the nacelle pressure distribution is changed, for instance, by the shroud number 1. Since according to measurement the shroud 1 reduces the mass flow and therefore according to [3] must have a positive natural circulation, additional velocities are induced at the nacelle tail which increase the static pressure as demonstrated by the pressure distribution.

2. Shroud. - The various shroud profiles which were investigated are taken from figure 7. The shrouds 1, 1a, and 1b differ only by the chord which was extended by a conically shaped metal piece. The shrouds 3, 3a, and 3b have the same profile, but different chord. For shrouds 5 to 5c the thickness ratio and the chord were

varied whereas the camber of the profile remained the same. The table reproduces the dimensionless values as well as the measured aerodynamic characteristic values of the single shrouds. Therein  $c_{wM}$  is the shroud drag measured for the condition with nacelle. By adding the amount  $\Delta c_{wG_1}$  to this value one obtains the actual parasite drag of the shroud  $c_{wM}$ . The values designated by \* are referred to the shroud development  $D_M \pi l_{Pr}$ . In the measured Reynolds number range a dependence on the characteristic values of the  $c_{wM}$  - values was hardly recognizable. One can count on more favorable values for the full-scale model, since the Reynolds number referred to the profile chord was at the most  $6.5 \times 10^7$ . This fact is of the highest importance for the attainable total efficiency as will be shown later. The drag coefficients ascertained for the shroud  $c_{wM}^*$  lie in the order of magnitude which is usual for plane wings. The net parasite drag of the shrouds is partly increased, partly reduced by addition of a nacelle. The dimensionless additional veloc-

ities  $\delta_0 = \frac{\bar{v}_{RS} - v}{v}$  given in the table as test values were determined by measurements of the velocity distribution over the radius. Figure 10 shows that the values  $\delta_{0th}$  calculated by D. Küchemann and J. Weber for several shrouds are on the average about 5 percent higher than the measured values. One can also well recognize from

the curve of the drag over  $1 + \delta_0 = \frac{\bar{v}_{RS}}{v}$  that the actual conditions approach theory most closely if the parasite drag  $c_{wM}^* \frac{l}{D}$  shows a minimum. This minimum lies at about  $1 + \delta_0 = 1.0$ , that is, in using profile shapes as were used here it is advisable, for instance, to equate the natural circulation of the shroud to zero in order to obtain small parasite shroud drags. However, the investigation was not sufficient to make a definite statement. Figure 11 shows how the axial velocity through the annular area is distributed over the radius for the arrangement "shroud - nacelle without propeller" in free stream. The velocity was measured, for instance, at the narrowest place of the shroud by a probe introduced from outside. For nearly all shrouds a considerable increase in velocity takes place toward the outside. Only the two shapes 1a and 1b differ in this respect because the great constriction of these shrouds at the nacelle tail causes such a large increase in pressure that the flow separates there. Altogether, it is essentially the total-pressure loss due to the friction along the nacelle surface which is responsible for the velocity reduction toward the hub (as shown by

the total-pressure measurements in figure 11). The total flow with and without propeller in motion was determined, as already mentioned, from these velocity measurements. Measurement results for the propeller in motion are given in a later figure. The pressure distribution at the shroud profile was measured on various shrouds. It is given in figure 12 for the shroud number 1 for a test with nacelle, without and with propeller. The propeller (number 1) was for these measurements set to  $\beta = 40^\circ$  at the tip. One can see that with decreasing ratio of advance, and therefore increasing loading, the loading of the shroud profile increases rapidly. The normal force coefficients  $c_{np_r}$  of the shroud profile given under the curves

which were approximately determined from the measured pressure distributions indicate the extent of the increase. These normal force coefficients are referred to the shroud profile chord and the stagnation pressure of the free stream velocity  $\frac{\rho}{2} v^2$ .

The  $c_{np_r}$  - values are according to definition positive if the normal force is directed inward, that is, if the incremental velocities  $\delta$  which are due to the shroud circulation are positive in the annular cross section. The position of the front stagnation point which shifts outward with increasing load can also be recognized from the pressure-distribution curves. The superstream velocities appearing at the outside of the shroud become negligible only for very high total loadings  $c_s$  ( $c_s > 6.0$ ). Since loads of this kind can hardly be considered at high speed, such a profile shape will be useless for very high flight velocities because of the then occurring compression shock.

Figure 13 shows for the shroud 1 the ratio of the axial flow velocity in the annular area at the radius  $r$  and the mean axial flow velocity in dependence on  $r/R$  for the cases "without propeller" and "with propeller" for various loadings  $c_s$ . The velocities were measured directly ahead of the propeller plane. One can recognize that by the influence of the static propeller the velocity distribution of the oncoming flow takes place more evenly. A

reduction of  $\frac{v_r}{\bar{v}_R}$  towards the hub becomes noticeable with increasing advance ratio;  $\frac{v_r}{\bar{v}_R}$  decreases the more the smaller the

propeller loading becomes. Since the pitch distribution of the propeller can be determined only for a particular distribution function  $v_r/\bar{v}_R = f(r/R)$ , one is forced to compromise. In order to eliminate the arising disadvantages regarding the factor of merit it will be expedient to fix the stator (if it is at all necessary) because of too high rotational losses) ahead of the propeller as an inlet stator and to impart a counter-rotation to the air. The changes

in inclination of the relative approach velocity toward the blade element of the propeller as compared to the plane of rotation are thereby reduced.

3. Propeller without shroud.- The coefficients of the propeller number 1 without shroud (with nacelle shape 1) are represented in figure 14 as functions of the advance ratio for several blade angles. The same figure shows also the thrust and power coefficients for static conditions ( $k_s^*$  and  $k_t^*$ ) and the static thrust factor of merit according to Bendemann

$$\zeta = \frac{k_s^*}{(2k_t^*)^{2/3}}$$

as functions of the blade angle.

In evaluating the total of measurements the parasite drags of the suspension as well as of the "nacelle alone" (without shroud, without propeller) were added to the measured thrust so that the coefficients indicated in the diagrams differ from those of the propeller alone solely by the drag of the nacelle which is increased because of the additional velocity of the propeller. The contribution of the pressure drag may therein assume a very considerable magnitude as will be discussed in more detail in the following section 4a. One can take

the efficiency ratio of the propeller  $\eta_{\text{measured}}$  from figure 15.

It is at the highest about 0.68. This unfavorable value is probably caused mainly by the high rotation losses and the shape of the blade tips which is unfavorable for use "without shrouding."

#### 4. Propeller number 1 in operation with shroud 1.-

(a) Without stator.- Figure 16 shows the aerodynamic coefficients of the propeller 1 with shroud 1 as functions of the advance ratio and of the blade angle of the propeller. One can see that the shrouding absorbs a very considerable part of the total thrust, particularly for static conditions. Moreover the propeller flow is, due to the natural circulation of the shroud, still sound at blade angles at which it would long since have separated without shroud. (See fig. 14.) Accordingly, the shrouding first improves essentially the static thrust factor of merit calculated by means of the Bendemann formula  $\zeta = k_s^*/(2k_t^*)^{2/3}$  and second makes an absolute magnitude of the static thrust coefficient  $k_s^*$  attainable which is more than twice as high as the one of the unshrouded propeller.

It is remarkable that for this arrangement the flow wetted completely the blunt afterbody (cap) (nacelle shape 1 according to figs. 1 and 9) due to the high exit rotation since the rotation which increased rapidly toward the axis caused very high negative pressure on the nacelle. Thereby the nacelle body experienced a very considerable pressure drag. The maximum efficiencies reached are small, corresponding to the large loss in rotation and pressure drag. The exit rotation was measured along the radius and the exit stator constructed accordingly.

(b) With exit stator.- The shape of the stator vanes can be taken from figures 1 and 5. They had to be fixed to the shroud because otherwise measurement of the reaction torque would have become impossible. The coefficients of the propeller 1 with shroud 1 and exit stator are shown in figure 17. The fact must be taken into consideration that the axial force of the stator itself is contained in the shroud thrust coefficient  $k_{SM}$ . According to expectation both maximum efficiency and static thrust factor of merit are essentially improved by the stator. Quite possibly the static thrust factor of merit calculated according to Bendemann will assume values over 1 because theoretically larger static thrusts can be obtained with a shrouded than with an unshrouded propeller. (Compare the deliberations of the section E II.) The maximum efficiency reached lies at around 0.70. It is mainly the natural drag of the shroud which is responsible for this small value as the considerations of the following sections E, I, and G will clearly demonstrate.

5. Propeller 1 four blades with exit stator and shroud number 1.- Figure 18 shows the coefficients of the shrouded four-blade propeller 1. Since the net propeller thrust decreases with the decreasing number of blades for equal advance ratio and equal blade angle the shroud thrust must also decrease. Due to the reduction of shroud circulation the additional velocity induced by the shroud in the propeller plane also decreases. Consequently the four-blade-propeller separates for smaller blade angles.

6. Propeller 2 with shroud 1 without and with exit stator.- Propeller 1 had been designed for uniform axial approach velocity along the radius. Propeller 2 differs from the former by only one specification: the twist was made smaller in order to take into consideration the tendency of the approach velocity distribution to increase toward the outside. The influence of this expedient can be seen in figures 19 and 20. For equal blade angle and equal advance ratio the values  $k_{SS}$ ,  $k_{SM}$ ,  $k_S$  and  $k_T$  are naturally smaller than for the propeller 1. However, the maximum efficiency is hardly changed. A slight improvement may be ascertained in the static thrust factor of merit. Therefore, the efficiency ratio of the propeller does not seem to be too sensitive to the distribution of the approach.

7. Propeller 1 with shroud 5c without exit stator.- Shroud 5c differs from shroud 1 mainly by its smaller chord and smaller thickness ratio. Thereby the natural drag  $c_{wM}^* \frac{l}{D}$  is according to figure 7, reduced to a value 0.0034 as contrasted with 0.01 for shroud 1. Moreover, the additional velocity caused by the shroud is positive ( $\delta_o = 0.13$ ) for the shroud 5c whereas it was negative for shroud 1 ( $\delta_o = -0.055$ ). Therefore, the characteristics  $k_s, k_l = f(\lambda)$  must take a different course from the ones for shroud 1. They may be taken from figure 21. The variation of the total thrust coefficient  $\overline{K}_g$  with the advance ratio is compared with the one measured for shroud 1, for the same adjustment angle  $\beta$ , somewhat steeper throughout. This fact is due to the positive circulation of shroud 5c. The total thrust becomes zero already for a smaller advance ratio. True to expectation the maximum efficiency is, particularly for large advance ratios, considerably improved because of the small parasite shroud drags. (For  $\beta = 55^\circ$  by about 10 percent.) Unfortunately this arrangement could not be investigated with stator. If one assumes that the gain in thrust due to an added stator would equal exactly the one measured for shroud 1 (fig. 17), for instance, propeller 1 with shroud 5c and stator would reach for  $\beta = 55^\circ$  a maximum efficiency of 0.77. An improvement of the maximum efficiency can, therefore, doubtlessly be obtained by means of shroud shapes of small chord and small thickness ratio. However, this advantage is neutralized by an essential disadvantage concerning the magnitude of the static thrust unless special precautions are taken. A comparison of the absolute static thrust and the static thrust factor of merit of the shrouds 5c and 1 clarifies the loss for static conditions. The bad effect for static condition is caused by the appearance of separation phenomena in the flow about the rather pointed profile nose of the shroud 5c which, first, decrease the shroud thrust and, second, reduce the propeller thrust. The reduction of the propeller thrust then causes a further decrease in shroud circulation, therefore in shroud thrust. However, this difficulty can be surmounted by a simple measure.

8. Improvement of the static thrust - behavior of thin shrouds by a nose split ring.- The following aims can be attained by attaching an outward going split ring to the nose of the shroud profile:

(1) Separation phenomena at the shroud are avoided for static conditions.

(2) The blade setting at which the flow separates at the propeller blade can be increased very considerably. Thus one is in a position to absorb more power with good efficiency.

(3) The low pressures appearing at the inlet at the shroud profile nose can be absorbed by the split ring surface. The shroud circulation, that is, the shroud thrust, increases.

(4) The advantageous effect of the nose split ring can be retained with about the same power expenditure even for small advance ratios, because for flow impinging on the shrouded propeller provided with a nose split ring (in free stream) the stagnation point lies up to a critical loading coefficient exactly on the outer edge of the ring. Only when the loading coefficient further decreases, separation phenomena will appear at the outer surface of the shroud due to the inward travel of the stagnation point; then, of course, the parasite drag will be increased very considerably.

The measurement results on propeller 1 with shroud 5c and nose split ring are presented in the figures 22 to 24. Figure 22 shows the considerable increase of the total thrust for static conditions for various shapes of the split ring. It is remarkable that not the largest of the investigated rings proved most favorable but a ring with a diameter of about 1.20 to 1.25 D (D = diameter of the propeller). No more essential increases in thrust could be obtained for the investigated profile by rounding off the frontal area. However, a further improvement of the static thrust by about 10 percent could be obtained by lengthening the shroud chord by a sheet metal cylinder pushed out to the rear. A simple cylindrical shrouding with nose split ring also brought good results. The use of such a shroud should be appropriate in special cases that require utmost simplicity of manufacture, for instance, for motor sleds and boats. The highest static thrust coefficient measured was for this case  $\bar{k}_S^* = 0.3$  for a Bendemann static thrust factor of merit  $\xi = 0.85$ . For an unshrouded propeller, the maximum static thrust was according to figure 14 about  $k_S^* = 0.15$  for an efficiency ratio of  $\xi = 0.65$ . These figures prove beyond doubt the advantage of such a simple shrouding. It is important that the effect of the split ring is retained even when it is subdivided several times along the circumference (see the dashed line in fig. 22, at the right). Extending several flaps probably would permit a simpler construction.

The results without and with split ring for the most favorable case are represented again in figure 23. Figure 24 reproduces the measured characteristics as functions of the advance ratio. One can see that, for instance, for an angle of blade adjustment  $\beta = 40^\circ$  up to an advance ratio  $\lambda = 0.3$  the total thrust of the arrangement "with split ring" is larger than without split ring. The power coefficient is almost unchanged. Thus one could fully utilize the advantages of the split ring for the climb also, and retract only for higher flight velocity.

By means of a smoke method (hydrochloric acid - ammonia) the flow at the shroud with split ring was made visible. The photographs 25(a) to 25(c) illustrate the effect of the split ring very clearly. For the smallest  $\lambda = 0.07$  (almost static thrust condition) the stagnation point lies exactly on the outer edge of the split ring as shown in figure 25(c).

Summarizing the properties of the split ring one may say that this expedient permits the utilization of short thin shrouds for the flight at high speeds without deteriorating the behaviour for static conditions.

It should be noted here that also for the case of the two-dimensional wing very considerable improvements of the maximum lift coefficient  $c_{a_{max}}$  were obtained by use of a nose split flap. According to a measurement by W. Krüger [8] the maximum lift coefficient of a high speed profile with the maximum thickness at 60 percent of the chord was for the most favorable case increased by  $\Delta c_{a_{max}} = 0.72$ .

## E. THEORETICAL CONSIDERATIONS

The following considerations concerning the shrouded propeller without losses and the shrouded propeller subject to losses have the purpose of explaining the aerodynamics of such propulsion units in a generally valid manner and to recognize what limiting values (efficiency, static thrust, etc.) are obtainable and what aspects must be heeded in order to obtain optimum values.

### I. Propeller in Forward Motion

1. Ideal case without energy losses.- From the change of momentum infinitely far in front of to infinitely far behind the propeller one obtains for flow without rotation the connection between the total thrust  $\bar{S}$ , the slipstream cross section  $F_{\infty}$  at infinity behind the propeller, the free stream velocity  $v$ , and the axial additional velocity in the jet  $w_a$  at infinity behind the propeller.

$$\bar{S} = \rho F_{\infty} (v + w_a) w_a$$

With  $\bar{S} = \bar{c}_s \frac{D}{2} v^2 F$  and  $\alpha = \frac{F_{\infty}}{F}$  the loading ratio becomes:

$$\bar{c}_s = 2\alpha \left( 1 + \frac{w_a}{v} \right) \frac{w_a}{v} \quad (1)$$

Thus the additional velocity to be ascertained from this equation

$$\frac{w_a}{v} = \frac{1}{2} \left( \sqrt{1 + \frac{2}{\alpha} \bar{c}_s} - 1 \right) \quad (2)$$

is for the same loading ratio  $\bar{c}_s$  the smaller, the larger becomes the slipstream cross-section ratio  $\alpha$ . Since the axial additional velocity in the slipstream determines the maximum theoretical efficiency for the shrouded as well as for the standard propeller, it is necessary to know how the slipstream cross-section ratio  $\alpha$  depends on the loading ratio and the shape of the shroud.

From the continuity equation one obtains

$$\alpha = \frac{F_{\infty}}{F} = \frac{F_{RS}}{F} \frac{\bar{v}_{RS}}{v + w_a} = \frac{F_{RS}}{F} \frac{1 + \delta_g}{1 + \frac{w_a}{v}}$$

Therein  $F_{RS} = F(1 - v^2)$  represents the annular cross section in the propeller plane,  $F = \frac{D^2 \pi}{4}$  the propeller disc area, and  $\delta_g = \frac{\bar{v}_{RS} - v}{v}$  the additional velocity in the propeller plane caused by the shroud and the propeller, referred to the free-stream velocity.

Furthermore, according to Bernoulli's energy equation,

$$\frac{w_a}{v} = \sqrt{1 + c_{sS}} - 1 \quad (3)$$

Thus one obtains for the slipstream cross-section ratio the relation:

$$\alpha = \frac{F_{RS}}{F} \frac{1 + \delta_g}{\sqrt{1 + c_{SS}}} \quad (4)$$

The additional velocity in the propeller plane caused by the shroud circulation and the propeller loading, referred to the free-stream velocity can be divided up (Kuchemann - Weber, [3]) according to definition as follows:

$$\delta_g = \frac{w_a}{2v} + \delta_o + \delta_S \quad (5)$$

$\delta_o$  represents the additional velocity of the shroud in free stream, caused by its circulation

$\delta_S$  additional velocity induced by an additional circulation corresponding to the propeller loading

$\delta_o$  therefore, is merely dependent on the shape of the shroud,  $\delta_S$  on the other hand, on the shape of the shroud and on the loading ratio  $c_{SS}$  of the propeller alone.

With the definition equation (5) and with equation (3), equation (4) may be written as follows:

$$\alpha = \frac{F_{RS}}{F} \frac{\frac{1}{2} \left( 1 + \sqrt{1 + c_{SS}} \right) + \delta_o + \delta_S}{\sqrt{1 + c_{SS}}} \quad (6)$$

Therefore, according to this equation the slipstream cross-section ratio for a given shroud shape ( $\delta_o$ ) and a given hub ratio  $\frac{F_{RS}}{F}$  is a function of the propeller loading ratio  $c_{SS}$  and of the additional velocity  $\delta_S$  caused by the additional circulation of the shroud. Since  $\delta_S$  increases with increasing propeller loading one may assume

that the influence of the propeller loading upon the slipstream cross-section ratio is very slight. This fact has already been pointed out by Weinig [9]. There the absolute magnitude of the cross-section ratio  $\alpha$  is brought into direct relation to the angle of inclination  $\delta$  of the trailing edge of the shroud profile toward the shroud axis:

$$\frac{F_{\infty}}{F} \approx \frac{F_A}{F} \frac{1}{1 - 0.45 \delta}$$

However, this relation can be applied only with great uncertainty when the profile trailing-edge angle is relatively large and if there is a hub body in the shroud.

Küchemann - Weber [3] calculated potential-theoretically the streamline picture for a loaded propeller with cylindric shroud. This exact calculation shows that for the cylindric shroud the slipstream cross-section ratio is not at all changed by the propeller loading as compared with the condition without propeller. Thus the assumption mentioned above is fully confirmed for this special case. The measurements and flow photographs given in section F of the present report also show essentially the same result. One may therefore assume with very great probability that a method of calculation for shrouded propellers based on a slipstream cross-section ratio that remains unchanged represents a good approximation which can be used for the technical design. The parallel between calculation and measurement drawn in section G confirms this assumption quite well.

The further considerations are based on the assumption that the slipstream cross-section ratio is not influenced by the loading ratio, but is determined merely by the shape of the shroud and the hub ratio of the propeller. Its magnitude must, therefore, be the same for all  $c_B$  values as in the case without loss for  $c_B = 0$ , thus "without propeller." Since for this case  $\delta_S = \delta_{oth}$  equation (4) appears in the simple form:

$$\alpha = \frac{F_{RS}}{F} (1 + \delta_{oth}) \quad (7)$$

Figure 26 represents the dependence of the slipstream cross-section ratio  $\alpha$  on  $\delta_{oth}$  and on the hub ratio  $v$ . If  $\delta_{oth}$  has not been calculated the slipstream cross-section ratio for any shape of shroud can be determined by flow measurement of the empty shroud with nacelle, without propeller. (Compare section F.) The power to be put in for the case without loss can be calculated from the kinetic energy which remains in the slipstream as

$$L = F_{\infty} (v + w_a) \rho \left[ \frac{(v + w_a)^2}{2} - \frac{v^2}{2} \right]$$

or with  $\bar{S} = \rho F_{\infty} (v + w_a) w_a$

$$L = \bar{S} v \left( 1 + \frac{w_a}{2v} \right) \quad (8)$$

From this equation one obtains the maximum theoretical efficiency of the shrouded propeller

$$\eta_m = \frac{1}{1 + \frac{w_a}{2v}} \quad (9)$$

and if one introduces the relation between the additional velocity, the total loading ratio and the slipstream cross-section ratio according to equation (2):

$$\eta_m = \frac{1}{1 + \frac{1}{4} \left( \sqrt{1 + \frac{2}{\alpha} c_B} - 1 \right)} \quad (10)$$

In figure 27  $\eta_m$  is represented as a function of the effective thrust loading ratio  $c_{s_e}$ . The diagram is valid for the case subject to friction and for the ideal case. For the ideal case  $\frac{c_{s_e}}{c_s} = c_s$ ; thus the effective thrust equals the thrust theoretically present for the same additional velocity  $w_a$ . The course of the maximum theoretical efficiency of the unshrouded propeller is drawn into the same diagram with a dashed line. One can see that the theoretical efficiency of the standard propeller for  $c_s \rightarrow 0$  approaches asymptotically the efficiency of the shrouded propeller with  $\alpha = 1$ , and for  $c_s \rightarrow \infty$  the efficiency of the shrouded propeller with  $\alpha = 0.5$ , as was to be expected. The considerations of W. Stuess [5] led to the same result.

The improvement of the theoretical efficiency by shrouding becomes considerable only for large slipstream cross-section ratios  $\alpha$ . However, the magnitude of the shroud circulation necessary for production of very considerable slipstream cross-section enlargements, when standard profile forms are used, can be obtained only at the price of very high shroud drags, in most cases the effective efficiency is thereby reduced beyond reasonable values.

In the following chapter the influence of losses upon the effect of the shrouded propeller is taken into consideration.

2. Shrouded propeller with energy losses taken into consideration.

The following considerations concern the shrouded propeller alone, that is, the drag of the nacelle (without propeller and without shroud) is not contributed to the propeller.

Due to the losses at the propeller and stator profiles the power input from the motor to the propeller must be larger than the power input from the propeller to the air flowing through. The power put into the propeller shaft will be designated by "induced power,"  $L_1$ . The losses at the profiles are for the standard propeller without shroud included by the factor of merit. Since the shape of the shrouded propeller is more like an axial blower we introduce instead of the factor of merit the blower efficiency  $\eta_G$  which is identical with it. Therefore, its definition is:

$$\eta_G = \frac{F_R v_R \Delta p_g}{L_1} \quad (11)$$

If one takes the equation (8) into consideration, the induced power will be

$$L_1 = \frac{1}{\eta_G} \bar{S} v \left( 1 + \frac{w_a}{2v} \right) \quad (12)$$

For the same induced power the effective thrust  $\bar{S}_e$  is, as compared with the theoretical  $\bar{S}$  of the propeller without loss; reduced by the magnitude of the drags  $W$ . The total drag consists of the parasite drag of the shroud  $W_M$  which appears for the condition without propeller, and of the additional drag  $\Delta W$  which is caused on shroud and nacelle by the additional velocities for the condition of a propeller in motion. Thus one obtains for the effective propulsive power:

$$L_e = (\bar{S} - W_M - \Delta W) v \quad (13)$$

so that the efficiency results from (12) and (13):

$$\eta = \eta_G \frac{\bar{S} - W_M - \Delta W}{\bar{S} \left( 1 + \frac{w_a}{2v} \right)}$$

If one refers the drags as well as the thrusts to  $\frac{\rho}{2} v^2 F$  and takes the magnitude of the maximum theoretical efficiency according to equation (9) into consideration, the obtainable total efficiency of the shrouded propeller alone can be written in the form:

$$\eta = \eta_m \times \eta_G \times \eta_{Ma} \times \eta_E \quad (14)$$

The separate efficiencies in this equation are defined as follows:

$$\eta_m = \frac{1}{1 + \frac{w_a}{2v}} \quad \text{maximum theoretical efficiency}$$

$$= \frac{1}{1 + \frac{1}{4} \left( \sqrt{1 + \frac{2}{\sigma} C_{Se}} - 1 \right)}$$

$$\eta_G = \frac{F_R \bar{v}_R \Delta p_g}{L_1} \quad \text{blower efficiency or factor of merit of the propeller (stator included)}$$

$$\eta_{Ma} = \frac{1}{1 + \frac{c_{wM}}{\bar{c}_{s_e}}} \quad \text{shroud efficiency}$$

$$\eta_E = \frac{1}{1 + \frac{\Delta c_w}{\bar{c}_{s_e} + c_{wM}}} \quad \text{installation efficiency}$$

$\bar{c}_{s_e}$  in these expressions represents the effective total thrust loading. This effective total thrust loading is the thrust reduced by the magnitude of the parasite drag as compared with the theoretically possible thrust of the propeller without loss, for the same effective blower power. The maximum theoretical efficiency has already been discussed in section E I 1. If the right dimensions are selected the blower efficiency can assume values above 0.9. The shroud efficiency is of decisive importance for the possibility of application as was mentioned before ([3], [6]). The shroud efficiency is plotted over  $\bar{c}_{s_e}$  in figure 27 for various drag coefficients of the shroud. The drag coefficient is referred to  $\frac{\rho}{2} v^2 F$ . There is therefore an optimum total loading for each special shroud ( $\delta_0, \alpha, c_{wM}$ ) for which the product of efficiencies  $\eta_m \times \eta_{Ma}$  is a maximum. (For examples, see fig. 28.)

The first three separate efficiencies can be calculated relatively simply. In order to calculate the installation efficiency  $\eta_E$  the additional drag caused by the slipstream must be estimated.

3. Calculation of the additional energy loss caused by the additional velocities for propeller in motion.- This amount can be determined only approximately. However, a numerical calculation carried out later showed that the magnitude of the installation efficiency as compared with the other separate efficiencies normally is of hardly any importance at all.

One assumes for this approximation that only the energy losses  $\Delta p_v$  caused for the flow through the shroud by the inner shroud surface and the corresponding part of the nacelle surface are

influenced by the additional propeller velocity. If we equate

$$\frac{\Delta p_v}{\frac{\rho}{2} v^2} = \mu \quad \text{and} \quad \frac{\Delta p_v}{\frac{\rho}{2} \bar{v}_{R_{\max}}^2} = \mu_e, \quad \text{with } \bar{v}_{R_{\max}} \text{ representing the velocity}$$

in the minimum annular cross section  $F_{R_{\min}}$ ,  $\mu_e$  becomes for the shroud without propeller (subscript o), if the continuity is taken into consideration:

$$\mu_{e_o} = \mu_o \frac{1}{\left( F_{RS} / F_{R_{\min}} \right)^2 (1 + \delta_o)^2}$$

Generally the minimum annular cross section will lie in the propeller plane; therefore will be  $\frac{F_{RS}}{F_{R_{\min}}} = 1$ . Only for shroud shapes which narrow in front of or behind the propeller, the quotient  $F_{RS} / F_{R_{\min}}$  becomes larger than 1. If one equates the loss coefficient  $\mu_e$  for propeller in motion to  $\mu_{e_o}$  (without propeller), one obtains as the total-pressure loss for propeller in motion:

$$\Delta p_v = \mu_o \left( \frac{1 + \delta_g}{1 + \delta_o} \right)^2 \frac{\rho}{2} v^2$$

Thus the additional total-pressure loss caused by the additional velocities is:

$$\Delta p_{v_{\text{jet}}} = \mu_o \frac{\rho}{2} v^2 \left[ \left( \frac{1 + \delta_g}{1 + \delta_o} \right)^2 + 1 \right] \quad (15)$$

$p_o = \frac{\Delta p_v}{\frac{\rho}{2} v^2}$  can be determined by flow measurements on the empty

shroud. With this total pressure loss according to equation (15) the loss power becomes:

$$\Delta L_{\text{Jet}} = F_{RS} (1 + \delta_g) \mu_o \frac{\rho}{2} v^3 \left[ \left( \frac{1 + \delta_g}{1 + \delta_o} \right)^2 - 1 \right]$$

If one equates  $\Delta L_{\text{Jet}} = \Delta c_w \frac{\rho}{2} v^3 F$ , there results as a good approximate value for the additional velocity, caused by the propeller in motion:

$$\Delta c_w = \frac{F_{RS}}{F} \mu_o (1 + \delta_g) \left[ \left( \frac{1 + \delta_g}{1 + \delta_o} \right)^2 - 1 \right] \quad (16)$$

The additional drag is, therefore, dependent on the total through flow  $(1 + \delta_g)$ ; this total through flow, however, is a function of the actual loading  $\bar{c}_{s1} = \bar{c}_{se} + c_{wM} + \Delta c_w$ , which shall be designated as induced loading; taking the equation (2) into consideration there results from the law of continuity for the additional velocity in the slipstream:

$$\frac{\bar{v}_{RS}}{v} = 1 + \delta_g = \alpha \frac{F}{F_{RS}} \frac{1}{2} \left[ 1 + \sqrt{1 + \frac{2}{\alpha} (\bar{c}_{se} + c_{wM} + \Delta c_w)} \right] \quad (17)$$

The comparison between calculation and measurement performed in section G shows that the influence of  $\Delta c_w$  upon the total through flow is noticeable only for very small advance ratios and even there is very slight. (See fig. 34.) Thus one is justified in writing for the installation efficiency in a first approximation:

$$\eta_E = \frac{1}{1 + \frac{\mu_0}{\bar{c}_{se} + c_{wM}} f(c)} \quad (18)$$

with

$$f(c) \approx \frac{1}{2\alpha} \left[ 1 + \sqrt{1 + \frac{2}{\alpha} (\bar{c}_{se} + c_{wM})} \right]$$

$$\left( \frac{\left[ \frac{F}{F_{RS}} \frac{\alpha}{2} \left[ 1 + \sqrt{1 + \frac{2}{\alpha} (\bar{c}_{se} + c_{wM})} \right] \right]^2}{1 + \delta_0} \right) - 1$$

One can obtain a second approximation if one calculates  $(1 + \delta_g)$  first from (17), neglecting  $\Delta c_w$ , and then determines the first approximation  $\Delta c_w(1)$  from (16) with this value. By inserting  $\Delta c_w(1)$  again into (17) one obtains the second approximation  $(1 + \delta_g(2))$  and therewith from (16) the second approximation  $\Delta c_w(2)$ . With  $\Delta c_w(2)$  the second approximation of the shroud efficiency according to (14) can be calculated.

Figure 29 represents the dependence of the installation efficiency  $\eta_E$  (calculated according to this method) on  $\bar{c}_{se} + c_{wM}$  for the parameters  $\alpha$  and  $p_0$ . According to figure 29 the influence of the pressure coefficient  $p_0$  upon the installation efficiency is of essential importance for large values of  $p_0$ . However, aerodynamically bad shroud forms must be a priori excluded for the design since large values of  $p_0$ , thus large  $c_{wM}$ , are connected with a bad shroud efficiency  $\eta_{Ma}$ . The test values for the pressure loss coefficient  $p_0$  given in section F show that this coefficient reaches for good shroud profiles a magnitude which guarantees very good installation efficiencies. A comparison of the curves for  $\alpha = 1$  and  $\alpha = 2$  demonstrates that the installation efficiency improves, for the same pressure loss coefficient  $p_0$ , with increasing slipstream cross-section ratio.

However, one must bear in mind that a larger slipstream cross-section ratio can be obtained only by larger intrinsic circulation and that therewith the losses  $(c_{wM}, \mu_0)$  also increase.

The influence of energy losses upon the total efficiency of the shrouded propeller was treated above. Thus one is in a position to calculate the obtainable maximum efficiency for any arrangement beforehand in a good approximation.

Knowledge of the mass flow and the total-pressure jump which is to be put in by the propeller is necessary.

4. Calculation of the mass flow flowing through the propeller.- The relation between the axial flow velocity through the propeller plane, the loading and the properties of the shroud was already indicated in equation (17). This relation yields the mass coefficient  $\varphi = \bar{v}_{RS}/u$  which can be directly taken over:

$$\varphi = \frac{\bar{v}_{RS}}{u} = \lambda \alpha \frac{F}{F_{RS}} \frac{1}{2} \left[ 1 + \sqrt{1 + \frac{2}{\alpha} (c_{se} + c_{wM} + \Delta c_w)} \right] \quad (19)$$

It has already been pointed out that the influence of the drag  $\Delta c_w$  caused by the additional velocity on the total through-flow is very slight. Thus one obtains a good first approximation from:

$$\varphi \approx \lambda \alpha \frac{F}{F_{RS}} \frac{1}{2} \left[ 1 + \sqrt{1 + \frac{2}{\alpha} (c_{se} + c_{wM})} \right] \quad (20)$$

For a more accurate calculation, in particular for a very small ratio of advance, one can proceed as follows: first  $(1 + \delta_g)$  is calculated in a first approximation from equation (17) (with  $\Delta c_w = 0$ ), with this value  $\Delta c_w$  is then determined from equation (16), and therewith  $\varphi$  as second approximation from equation (19).

5. Calculation of the pressure jump to be established.- According to the consideration in section E I 1 the power input from the propeller to the air flowing through is determined by the kinetic

energy remaining in the slipstream. The magnitude of this power is according to equation (8) written in a slightly different manner:

$$L = \left( \bar{c}_{se} + c_{wM} + \Delta c_w \right) \frac{\rho}{2} v^3 F \left( 1 + \frac{w_a}{2v} \right)$$

On the other hand it is to be explained as blower feed performance:

$$L = Q \times \Delta p_g = F_{\infty} v \left( 1 + \frac{w_a}{v} \right) \Delta p_g$$

Taking the relation for the additional velocity

$$\frac{w_a}{v} = \frac{1}{2} \left[ \sqrt{1 + \frac{2}{\alpha} \left( \bar{c}_{se} + c_{wM} + \Delta c_w \right)} - 1 \right]$$

of the equation (2) into consideration one obtains from the two above equations the pressure coefficient of the blower

$$\psi = \frac{\Delta p_g}{\frac{\rho}{2} u^2}$$

$$\psi = \lambda^2 \frac{\bar{c}_{se} + c_{wM} + \Delta c_w}{2\alpha} \left[ \frac{3 + \sqrt{1 + \frac{2}{\alpha} \left( \bar{c}_{se} + c_{wM} + \Delta c_w \right)}}{1 + \sqrt{1 + \frac{2}{\alpha} \left( \bar{c}_{se} + c_{wM} + \Delta c_w \right)}} \right] \quad (21)$$

7. The operating condition of the propeller for varying ratio of advance.- The proportional number customary in blower construction

$$\sigma = \frac{\rho \bar{v}_{RS}^2}{\Delta p_g} = \frac{\phi^2}{\psi}$$

is characteristic for the operating condition with respect to flow mass and pressure jump. For the standard propeller without shroud  $\sigma$  varies very considerably in the region of the ratio of advance  $\lambda = 0$  to  $\lambda = \lambda_{max}$ ,  $\sigma$  increases with growing  $\lambda$ , that is, the propeller blade is not loaded. However, the propeller can only work for a quite definite operating condition ( $\sigma$ ), namely for the design condition for the most favorable efficiency. If the operation condition varies very greatly with the ratio of advance,  $\eta$  decreases; moreover, sometimes the blade must be made adjustable. Due to the change in circulation at the shroud profile for varying ratio of advance additional velocities are induced in the propeller plane for the shrouded propeller whose effect makes the operating condition of the propeller for the entire region of advance ratio change very much less than for the standard propeller. If one would succeed in constructing the shroud in such a manner that  $\sigma$  remains the same for the entire  $\lambda$  - region, one would gain two essential advantages:

1. The propeller would not have to be adjustable,
2. The blower efficiency and the propeller efficiency ratio would equal the maximum value at the design point for the entire  $\lambda$  - region.

From the relations found for the mass coefficient  $\phi$  (equation (19)) and the pressure coefficient  $\psi$  (equation (21)) one obtains

$$\sigma = \frac{\rho \bar{v}_{RS}^2}{\Delta p_g} = \frac{\alpha^3 \left(\frac{F}{F_{RS}}\right)^2 \left[1 + \sqrt{1 + \frac{2}{\alpha} (\bar{c}_{se} + c_{wM} + \Delta c_w)}\right]^3}{2(\bar{c}_{se} + c_{wM} + \Delta c_w) \left[3 + \sqrt{1 + \frac{2}{\alpha} (\bar{c}_{se} + c_{wM} + \Delta c_w)}\right]} \quad (22)$$

Figures 30(a) and 30(b) show the dependence of the operating condition  $\sigma$  on the induced loading  $\bar{c}_{s_e} + c_{w_M} + \Delta c_w$  for various slipstream cross-section ratios  $\alpha$ , that is, for various shapes of the shroud.

The corresponding curve for the propeller without shroud is also plotted in figure 30(a). The curves are valid for a hub ratio  $\nu = D_{hub}/D = 0.25$ . They clearly show the advantage of the shrouded propeller. On the other hand one can see that the goal of equal operating condition in the entire  $\bar{c}_s$  - region can not be reached by means of one and the same shape of shroud. In order to really reach this aim  $\alpha$ , that is, the circulation of the shroud would have to be variable during the flight. This condition can be fulfilled only by changing the form of the profile (for instance flaps) or by influencing the boundary layer at the shroud profile [10]. Figure 30(b) shows that the presence of a hub changes the tendency of the curves only slightly.

The following chapter contains a few considerations of the behavior of the shrouded propeller at rest.

## II. Propeller at Rest

All values referred to the static thrust condition are designated by an asterisk\*.

1. Ideal case without energy losses.— A consideration of the momentum yields the magnitude of the static thrust for irrotational outflow:

$$\bar{S}^* = \alpha F w_a^{*2} \quad (23)$$

Just as in the case of the propeller in forward motion the power to be put in equals the kinetic energy lost per second:

$$L^* = \alpha F \frac{\rho}{2} w_a^{*3} = \bar{S}^* \frac{w_a^*}{2} \quad (24)$$

From (23) and (24) one obtains the connection between the static thrust and the power to be put in for the theoretical case without friction:

$$\bar{S}^* = (\rho \alpha F)^{1/3} (2L^*)^{2/3} \quad (25)$$

If one equates

$$\bar{k}_S^* = \frac{\bar{S}^*}{\frac{\rho}{2} u_F^2}$$

$$\bar{k}_L^* = \frac{L^*}{\frac{\rho}{2} u_F^3}$$

one can write dimensionlessly:

$$\bar{k}_S^* = 2\alpha^{1/3} \bar{k}_L^*{}^{2/3} \quad (26)$$

Of course, this relation is also valid for the special case of the propeller without shroud. Since here  $\alpha = \frac{1}{2}$ ,  $\bar{k}_S^*$  without shroud becomes

$$\bar{k}_S^* \text{ without shroud} = (2\bar{k}_L^*)^{2/3}$$

Thus the static thrust coefficients with and without shroud are in direct ratio to

$$\bar{k}_S^* / \bar{k}_S^* \text{ without shroud} = (2\alpha)^{1/3} \quad (27)$$

The physical limits of the obtainable static thrust for standard propellers have been treated in detail by A. Betz [1].

It is theoretically possible to increase the absolute magnitude of the static thrust for the same power input to any degree by the use of a shroud if one succeeds in making the slipstream cross-section ratio sufficiently large by a shroud with large circulation. Practically, however, this possibility is limited, if simple profiles are used, because of the energy losses which appear in the diffuser behind the propeller. Probably these limits can be considerably shifted upward by special expedients, for instance, influencing of the boundary layer at the shroud profile. Experiments by B. Rezenscheid [10] on a nozzle with suction at the trailing edge have shown that even without geometrical diffuser considerable through-flow variations can be obtained by the suction. This behavior was to be expected after the experiences with trailing-edge suction on plane wings.

The static thrust factor of merit of the shrouded propeller is with (26):

$$\zeta_u = \frac{\bar{k}_{s_e}^*}{\bar{k}_s^*} = \frac{\bar{k}_{s_e}^*}{2\alpha^{1/3} k_t^{*2/3}} \quad (28)$$

$\bar{k}_s^*$  represents the theoretically obtainable total static thrust whereas  $\bar{k}_{s_e}^*$  represent the total static thrust actually obtained with the same power input.

2. Shrouded propeller at rest with energy losses taken into consideration. - The power necessary for production of the effective thrust  $\bar{S}_e^* = \rho \alpha F w_a^{*2}$  (equation (23)) is distinguished from the power calculated theoretically according to (24) first by the additional power to be put in because the energy transfer from the propeller to the air flowing through is subject to losses and second by the amount of power which has to cover the losses  $\Delta p_v^*$  originating in the flow through the shroud. The induced power necessary at the propeller shaft then is:

$$L_1^* = \frac{1}{\eta_G^*} \alpha F \frac{\rho}{2} w_a^{*3} \left( 1 + \frac{\Delta p_v^*}{\frac{\rho}{2} w_a^{*2}} \right) = L^* \frac{1 + \frac{\Delta p_v^*}{\frac{\rho}{2} w_a^{*2}}}{\eta_G^*} \quad (29)$$

Since according to equation (25) the total static thrust  $\bar{S}^*$  is related to the power  $L^{*2/3}$ , one obtains as the reachable static thrust factor of merit of the shrouded propeller:

$$\zeta_u = \left(\frac{L^*}{L_1^*}\right)^{2/3} = (\eta_G^* \eta_E^*)^{2/3} \tag{30}$$

with the installation factor of merit for static condition

$$\eta_E^* = \frac{1}{1 + \frac{\frac{\rho}{2} w_a^2}{\Delta p_v^*}} = \frac{1}{1 + \frac{\Delta p_v^*}{\frac{\rho}{2} \bar{v}_{R_{max}}^2} \alpha^2 \left(\frac{F}{F_{R_{min}}}\right)^2}$$

The actually obtainable static thrust then has the magnitude:

$$\bar{k}_{S_e}^* = \zeta_u \bar{k}_S^* = (\eta_G^* \eta_E^*)^{2/3} 2\alpha^{1/3} k_l^{*2/3} \tag{31}$$

From this dependence one can clearly see how greatly the obtainable static thrust is influenced by the installation factor of merit. The theoretical static thrust must increase with growing slipstream cross-section ratio  $\alpha$ . On the other hand the installation factor of merit  $\eta_E^*$  decreases with growing  $\alpha$ . Since the loss coefficient

$\frac{\Delta p_v^*}{\frac{\rho}{2} \bar{v}_{R_{max}}^2}$  also will increase with growing  $\alpha$ , that is, for shrouds

becoming enlarged, it is to be expected that  $\eta_E^*$  decreases very sharply. For this reason the static thrust could not be essentially increased further by use of further enlarged shrouds as compared with approximately cylindric ones in the tests carried out so far. The hub also has an unfavorable influence on the obtainable static thrust because the installation factor of merit also deteriorates with increasing hub diameter.

Figure 31 shows the dependence of the value  $\overline{k_{se}}^*/(2k_v^*)^{2/3}\eta_G^{*2/3}$  on the slipstream cross section ratio  $\alpha$  and on the loss coefficient  $p_e^* = \frac{\Delta p_v^*}{\frac{\rho}{2} v_{R_{max}}^*2}$  for two hub ratios  $F_{R_{min}}/F = 1$  and  $F_{R_{min}}/F = 0.75$  corresponding to  $\frac{D_{hub}}{D} = 0$  and  $0.5$ , respectively. The influence of the installation factor of merit  $\eta_E^*$  on the static thrust becomes even more evident if one inserts the loss into equations (30) and (31) in the form  $\Delta p_v^* = (1 - \eta_D) \frac{\rho}{2} (\overline{v_{P_{max}}}^2 - w_a^2)$  with  $\eta_D$  representing the diffuser efficiency. As the result of this calculation the function of figure 31 is again plotted in figure 32, but with the diffuser efficiency as parameter. Since this latter will hardly increase beyond 0.9 unless special steps are taken one can see that an attempt to increase the slipstream cross-section ratio essentially beyond  $\alpha = 1$  would be useless.

F. ADDITIONAL MEASUREMENTS CONCERNING THE PROBLEM OF THE  
SLIPSTREAM CROSS SECTION AND THE PRESSURE LOSSES  
IN THE FLOW THROUGH THE SHROUD

I. Slipstream Cross-Section Ratio  $\alpha$

In order to check the independence of the slipstream cross-section ratio  $\alpha = \frac{F_{co}}{F}$  of the loading presumed in section E several further measurements on shroud 1 were performed. For this shroud the slipstream cross-section ratio for the theoretical case (no energy added or removed during the flowing through the shroud) is according to equation (7):

$$\alpha = \frac{F_{RS}}{F} (1 + \delta_{oth}) = 0.878$$

for shroud 1:  $\delta_{oth} = 0$  (fig. 7) and  $F_{RS}/F = 0.878$ .

For the two limiting cases "shroud without propeller" and "shroud with propeller for static thrust condition" the slipstream cross-section ratio  $\alpha$  can be calculated from the mass flow and the mean total pressure in the exit cross section of the shroud according to the method described below; thus one can determine how far the presumption of a cross-section ratio remaining unchanged has actually been fulfilled.

The continuity yields:  $\alpha = \frac{F_R}{F} \frac{\overline{v_R}}{v_\infty}$ .

For the two limiting cases the mean axial flow velocity through the propeller disc area was determined by measurement. Under the assumption that the energy of the jet is not varied any further behind the exit cross section of the shroud, the slipstream velocity far behind the propeller can be calculated from Bernoulli's energy equation:

$$v_\infty = \sqrt{\frac{2}{\rho} (\overline{p}_{gA} - p_{St0})}$$

In this equation

$\overline{p}_{gA}$  mean total pressure in the exit cross section  $F_A$

$p_{St0}$  static pressure far behind the propeller. This pressure has to be equated to the static pressure in the undisturbed flow

The mean total pressure  $\overline{p}_{gA}$  in the exit cross section also was measured for both limiting cases.

The numerical result for shroud 1 is:

Theoretically, without change in energy . . . . .	$\alpha = 0.878$
Measurement, without propeller . . . . .	$\alpha \approx 0.890$
Measurement, with propeller 2 ( $\beta = 40^\circ$ ), with stator at rest $\lambda \approx 0$ . . . . .	$\alpha \approx 0.94$

It is to be expected that  $\left(\frac{F_\infty}{F} - 1\right)$  somewhat increases with increasing loading, in particular for shrouds with enlarged rear portion. The shroud which was examined here more closely is behind the propeller plane about cylindric, its circulation is almost zero and the variation of the slipstream cross-section ratio  $\alpha$  with the loading is very small. The absolute magnitude of the cross-

section ratio  $\alpha$  agrees quite well on the average with the theoretical magnitude of the empty shroud.

With the aid of the smoke method already mentioned in section D it was attempted to make the jet boundaries for various loadings of the propeller visible. Figure 33 shows that increasing propeller loading, in fact, causes hardly any variation of the jet contour. Unfortunately, the slipstream cross-section ratio could not be checked for more greatly enlarged shrouds because there was no stator for these shrouds. The large exit-rotation renders a comprehensive photograph impossible.

## II. Pressure Losses in the Flow Through the Shroud

According to the considerations of section E the pressure loss  $\Delta p_{v_0}$  which originates in the flow through the shroud (without propeller) is of essential influence on the magnitude of the installation efficiency  $\eta_E$ . Figure 29 showed the dependence of the installation efficiency on the loading, the slipstream cross-

section ratio, and the loss coefficient  $p_0 = \frac{\Delta p_{v_0}}{\frac{\rho}{2} v^2}$ . It is

interesting to ascertain the order of magnitude of this loss coefficient  $p_0$  for the shrouds investigated. To this end the mean total pressure shortly in front of and shortly behind the shroud for several extreme shroud shapes was determined by measurement, taking into consideration only the mass flowing through the shroud.

The following numerical values resulted for the three investigated shroud shapes 1, 5c, 7:

$$\text{shroud 1} \quad p_0 = 0.010$$

$$\text{shroud 5c} \quad p_0 = 0.007$$

$$\text{shroud 7} \quad p_0 = 0.180$$

If one considers the curves  $\eta_E = f(c_S)$  that are valid for these  $p_0$  - values (fig. 29) one can see that the installation efficiency for the first two shrouds equals almost 1 whereas it deviates from 1 considerably for shroud 7 which has a very strong diffuser. The effects of large mass flow losses, that is, of large  $p_0$  - values on the static thrust show according to calculations and to measurements the same tendency.

G. COMPARISON BETWEEN CALCULATION AND MEASUREMENT

With the aid of the exhaustive measurements which were in particular taken on the shroud 1 in connection with the propeller 2 and exit stator, the reliability of the calculation described in section E can be checked. The measured coefficients  $k_s$ ,  $k_l$ ,  $\eta$ , and  $\lambda$  are given in figure 20 as functions of the blade angle  $\beta$ . For three blade angles ( $40^\circ$ ,  $55^\circ$ ,  $65^\circ$ ) the mass coefficient  $\phi = \overline{v_{RS}}/u$  calculated according to equations (19) and (20), respectively, is represented as a function of the advance ratio  $\lambda$  in figure 34. The effective total thrust loading  $\overline{c_{se}}$  was determined for each blade angle and advance ratio considered from  $\overline{k_{se}}/\lambda^2$ . The parasite shroud drag of the shroud 1, with nacelle, results from the measurements. (See fig. 7.) The slipstream cross-section ratio could be determined from equation (7), since  $\delta_{oth}$  is known. Several test points, besides the calculated curves, are plotted in the diagram. (See fig. 34.) There is excellent agreement between calculation and measurement, in particular for the second approximation calculated from equation (20).

Figure 35 shows the dependence of the measured efficiency on the effective total thrust loading  $\overline{c_s}$  for three blade angles. Furthermore, the values for the maximum theoretical efficiency  $\eta_m$ , the shroud efficiency  $\eta_{Ma}$ , and the installation efficiency  $\eta_E$ , which were calculated according to section E, are plotted in the same diagram. Thus the product  $\eta_m \eta_{Ma} \eta_E$  represents the efficiency obtainable by calculation if the transfer of energy in the propeller would take place without loss ( $\eta_G = 1$ ). The ratio of the measured efficiency and the product of efficiencies  $\eta_m \eta_{Ma} \eta_E$  indicates the presumable magnitude of the blower efficiency  $\eta_G$ .  $\eta_G$  is represented as a function of  $\overline{c_s}$  in figure 36 and as a function of the ratio of advance in figure 37. For several  $\lambda$  and  $\beta$  the actually existing blower efficiency was approximately ascertained from the measurement. It can be determined from the ratio

$$\frac{\sum S_{wing}(\text{propeller} + \text{stator}) \overline{v_{RS}}}{L_{shaft}}$$

The shaft power  $L_{\text{shaft}} = k_7 \frac{\rho}{2} u^3 F$ , as well as the mean axial flow velocity through the propeller disk area were measured directly. The thrust effective on the propeller blades resulted from the measured thrust of propeller and nacelle plus nacelle drag. The pressure drag of the nacelle could be determined from pressure-distribution measurements. For calculating the propeller blade thrust it was assumed that the friction drag of the nacelle is small compared with the pressure drag. The experiences on profiles with large thickness ratio ( $>0.25$ ) and the maximum thickness far to the rear support this assumption.

The stator thrust was determined from the difference of the shroud thrust with and without stator. The blower efficiencies ascertained from the measurements according to this method are plotted in figure 37 as separate points for the three blade angles  $\beta = 40^\circ, 55^\circ, \text{ and } 65^\circ$ . The agreement with the rest-efficiency calculated from  $\eta_{\text{measured}}/\eta_m \eta_{Ma} \eta_E$  is not unsatisfactory if one considers the uncertainty in determining the blower efficiency from the measurement.

Since for shroud 1 according to the test results given in section F, the pressure loss which originates in the flow through the shroud, is also known, the calculation performed for the static case in section E II also may be compared with the test results. The installation factor of merit for static thrust conditions  $\eta_E^*$  to be calculated according to equation (30) has, for the shroud 1, the magnitude 0.988. It almost equals 1 because there is no strong diffuser present and thus no large losses can occur. With the blower efficiencies according to figure 37 which were determined directly from the measurement one obtains the following comparison:

$\beta$	$\xi = \frac{\bar{k}_s^*}{(2k_7^*)^{2/3}}$	$\eta_G^*$	$\xi_u = \frac{\bar{k}_s^*}{2\alpha^{1/3} k_7^* 2/3}$	$\xi_u = (\eta_G^* \eta_E^*)^{2/3}$
(deg)	From measurement (see fig. 20)	From measurement	From measurement	Calculation
40	1.035	0.765	0.860	0.830
55	.512	.220	.426	.370
65	.192	.087	.160	.200

If the values of the blower efficiency and of the pressure losses within the shroud are known, the static thrust obtainable can easily be calculated in advance.

#### H. SUMMARY AND CONCLUSIONS

In the present report test results on a shrouded propeller were given which was designed for high-speed flight and high-thrust loading. The measurements cover the entire region of advance ratios from 0 to  $\lambda_{\max} \approx 1.2$  and include the influences of variations in the form of propeller and shroud on the aerodynamic behavior of the shrouded propeller. Since the propeller is heavily loaded a stator is absolutely necessary in order to avoid the high rotational losses and the large pressure drag of the nacelle due to suction at the afterbody. The maximum efficiency measured is 0.71. The measurements permit the conclusion that the maximum efficiency could be essentially increased by using shroud forms of smaller chord and profile thickness. However, thin shroud profiles with small nose radius have a very unfavorable effect on the static thrust behavior. The static thrust factors of merit measured for large shroud chord (Bendemann  $\xi = \bar{k}_s^* / (2k_l^*)^{2/3}$ ) reach values over 1.1. The static thrust behavior can be improved very considerably by application of a nose split ring pointing outward on a shroud profile of small chord and thickness. The nose split ring permits, for static conditions and even for small ratios of advance, essentially larger propulsion powers to be converted with good efficiency into useful power than it is possible for a shrouded propeller without split ring. The absolute maximum value of the total static thrust is, according to the measurement, increased to more than twice the value as compared with the case "without" split ring. Thus it is possible to utilize by this expedient the advantages of short thin shroud profiles which are essential for high-speed flight, without deterioration of the static thrust behavior.

Subsequent to the given test results the shrouded propeller without and with energy losses is considered theoretically. These considerations are applied to both propeller in forward motion and propeller at rest. The calculations are based on the essential assumption that the slipstream cross section far behind the propeller depends only on the shape of the shroud, not on the loading of the propeller. The correctness of this assumption is supported by several additional measurements and by flow photographs at least for shrouds without large circulation. Therefrom results a simple possibility to calculate the properties of shrouded propellers in advance with a very good approximation and furthermore

to realize clearly the influence of energy losses on the aerodynamic behavior. The limits of efficiency attainable for propulsion units of this kind are thus made visible.

The shrouded propeller surpasses the standard propeller by essentially better static thrust factors of merit. The magnitude of the static thrust is limited by the losses originating in the flow through the shroud (mainly diffuser losses). Subsequently an attempt is made to increase the static thrust further by applying an influencing of the boundary layer at the shroud. Due to the parasite intrinsic drag of the shrouding the shrouded propeller will be particularly suitable for propulsion by pusher propeller because here the shroud could, circumstances permitting, simultaneously take over the function of the damping surfaces for the plane. For an airship body the possibility of stabilization by means of annular tail surfaces is confirmed by wind-tunnel measurements by R. Seiferth [11]. Its application is also very promising for other cases. Work on further development will have to aim mainly at a reduction of the parasite drag of the shroud alone for small superstream velocities at high speed. There is a possibility of success by use of laminar profiles. Thus the shroud would have to be designed for flight conditions at high speed and could be improved with respect to the magnitude of the static thrust by use of the nose split flap and, circumstances permitting, simultaneous steps for increase of the circulation in the rear domain of the profile.

The test results of the shroud profiles 1a, 1b, 2, 3, 3a, 3b, 4, 5, 5a, 5b, 6, 7, and 8 (fig. 7) which are not given in the present report are at the disposal of interested parties and be claimed at the AVA Göttingen.

Translated by Mary L. Mahler  
National Advisory Committee  
for Aeronautics

## K. REFERENCES

1. Betz, A.: Physikalische Grenzen des erreichbaren Standschubes, Jahrbuch 1938 der deutschen Luftfahrtforschung I, 348.
2. Regenscheit, B.: Standschubmessungen an 2 ummantelten Luftschauben. UM 681.
3. Kuchemann, D., and Weber, J.: Ueber die Strömung an ringförmigen Verkleidungen. FB 1236/7.
4. Hansen, M.: Standschubverbesserung durch Düsenring bei einer Modell-Luftschaube kleiner Steigung. UM 3043.
5. Stiess, W.: Erweiterte Strahltheorie für Düsen-schrauben mit um ohne Leitapparat. Werft, Reederei, Hafen 1936, Heft 14 and 15.
6. Pabst, O.: Die Berechnung ummantelter Schrauben. Focke-Wulf - Bericht GDV Nr. 20.
7. Betz, A.: Diagramme zur Berechnung von Flügelreihen. Ingenieurarchiv II, 1931, p. 359.
8. Krüger, W.: Ueber eine neue Möglichkeit der Steigerung des Höchstauftriebes von Hochgeschwindigkeitsprofilen. UM 3049.
9. Weinig, F.: Aerodynamik der Luftschaube. Berlin, Verlag J. Springer 1940, p. 323 ff.
10. Regenscheit, B.: Venturidüsen mit veränderlichem Durchfluss. (also available as NACA TM No. 1191.)
11. Seiferth, R.: Wind Tunnel Tests on a 1/75-Scale Model of the Goodyear - Zeppelin Airship Akron Z.R.S.4 with Normal and Ring Tail Surfaces. Report No. 105 of the Guggenheim Aeronautics Laboratory, California Institute of Technology.

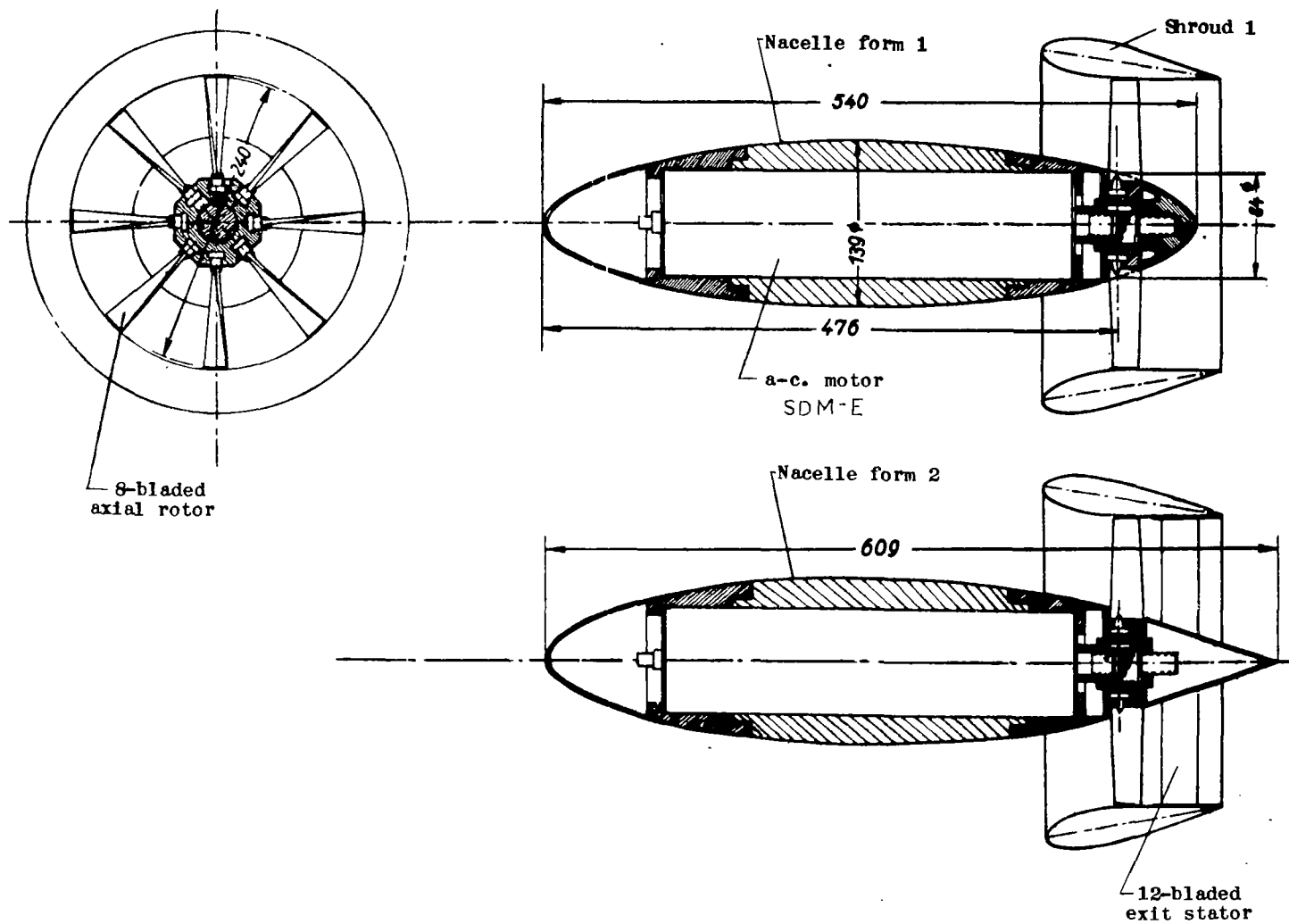


Figure 1.- The investigated model of the shrouded propeller. Scale 1:5.

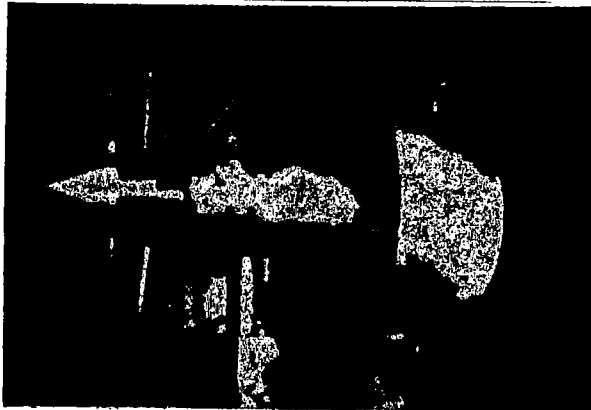


Figure 2.- Oblique front view.



Figure 3.- View of the stator.

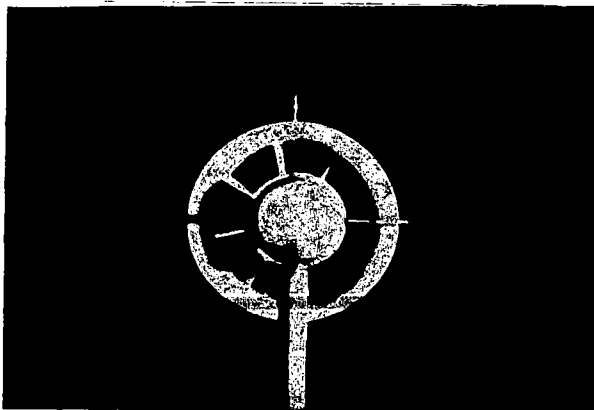
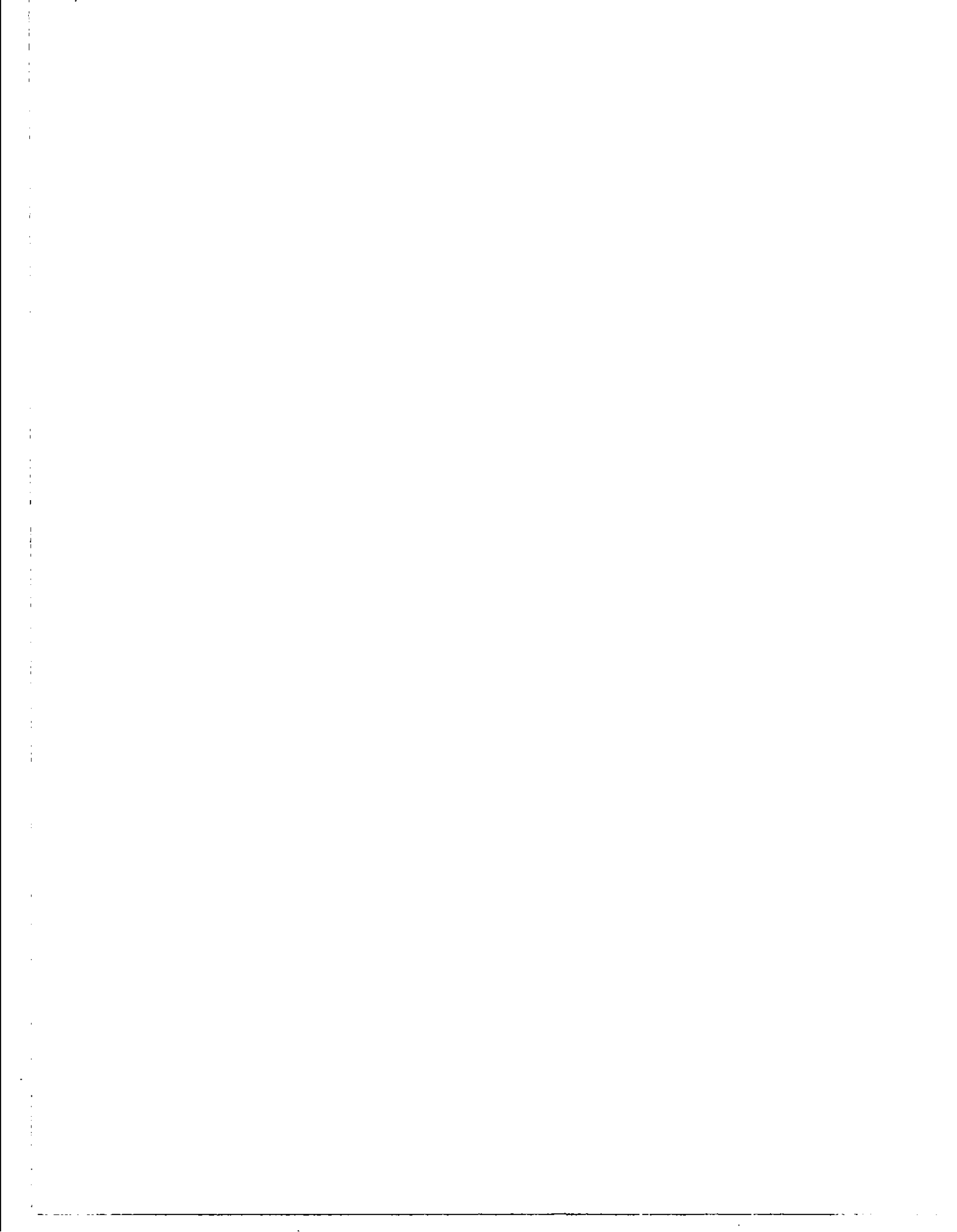


Figure 4.- View in flow direction.

Figures 2-4.- Views of the model (shroud 1) in the wind tunnel.



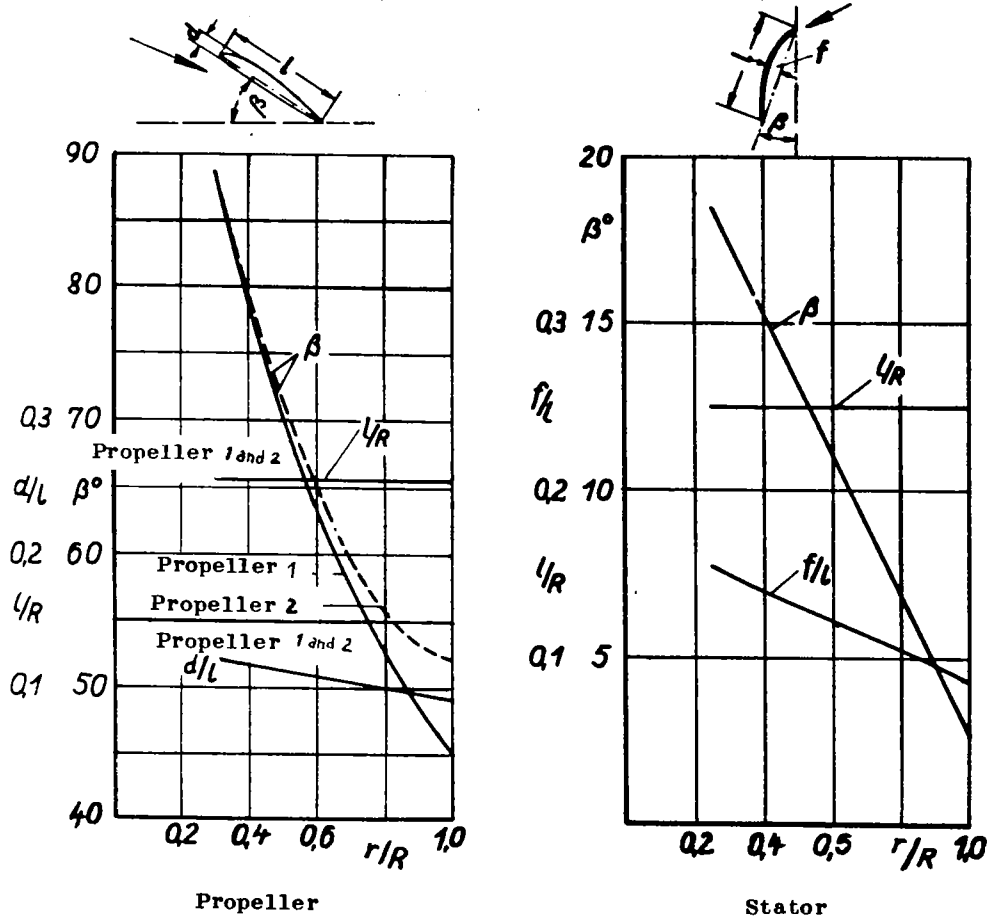
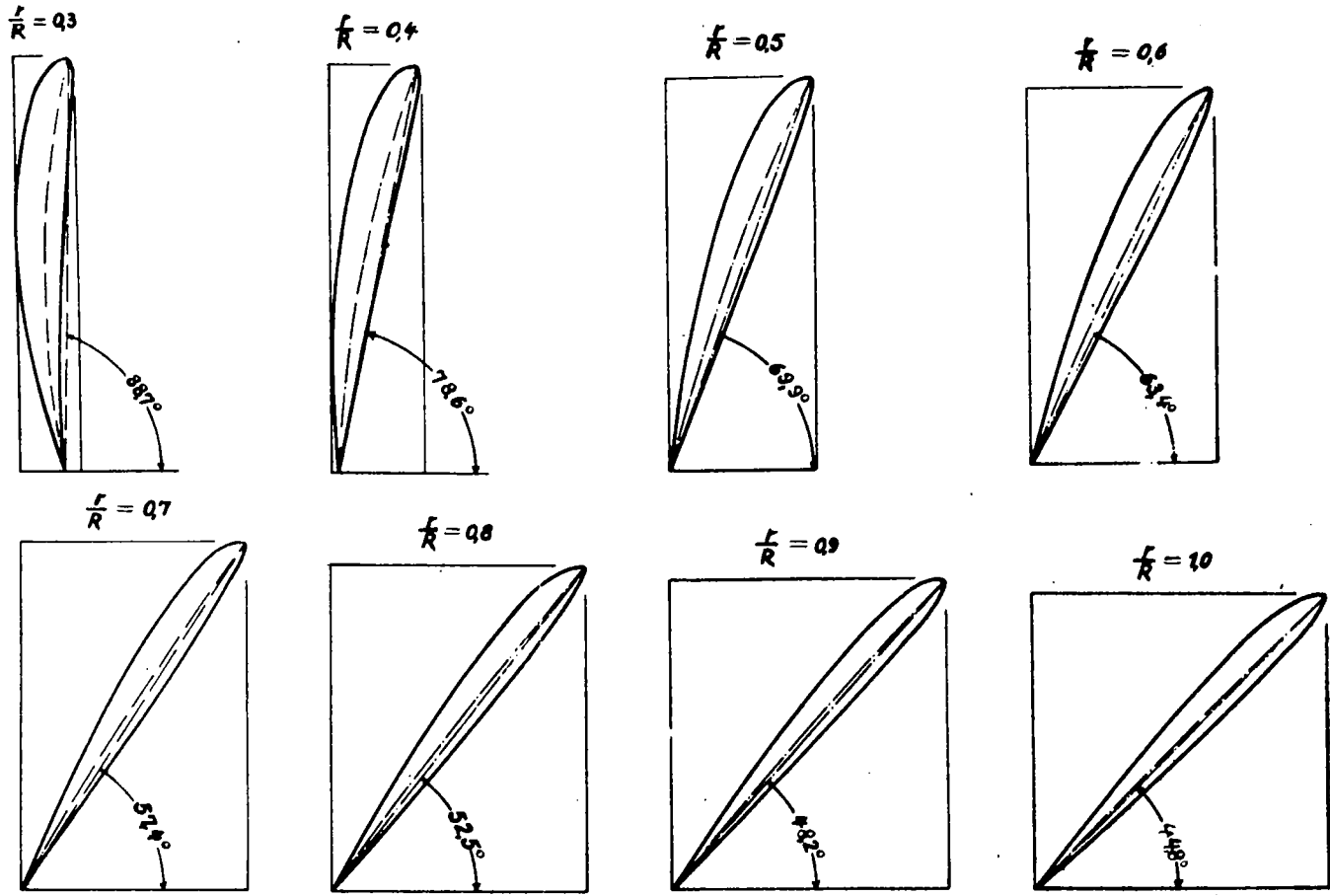
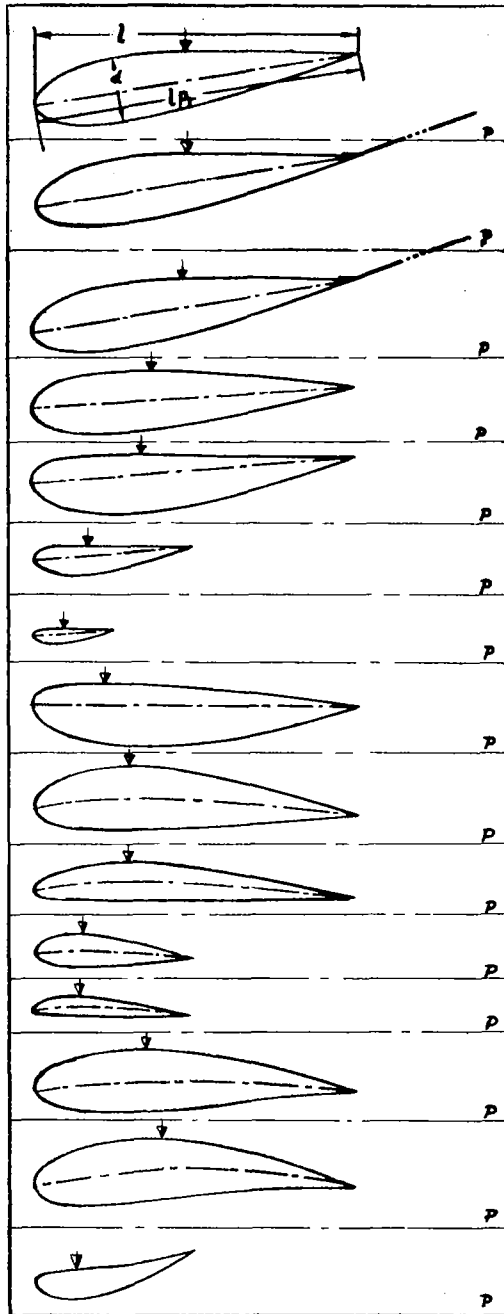


Figure 5.- Dimensions of the propeller and stator blades.



$R = 120 \text{ mm}$

Figure 6.- Profiles of the propeller blade. Scale of the drawing 2:1. Blade angles are valid for propeller No. 1.



Shroud No.	l/D	d/LP	F/F	C <sub>w</sub> nacelle		C <sub>w</sub> M		C <sub>w</sub> M		C <sub>w</sub> M		δ <sub>0</sub>	δ <sub>th</sub>
				with	without	with	without	with	without				
1	0.625	0.200	2.63	0	0.046	-0.046	0.091	0.045	0.016	0.059	0.021	-0.055	0
1a	0.872	-	3.87	-0.107	0.046	-0.153	0.286	0.133	0.036	-	-	-0.428	-
1b	1.170	-	4.18	-0.104	0.046	-0.150	0.308	0.238	0.057	-	-	-0.716	-
2	0.625	0.195	2.79	0.088	0.046	0.042	0.006	0.048	0.077	0.047	0.077	0.140	0.200
3	0.625	0.195	2.68	0.013	0.046	-0.033	0.098	0.065	0.024	0.005	0.024	-0.030	0
3a	0.312	0.195	1.31	0.029	0.046	-0.077	0.050	0.033	0.025	0.042	0.032	-0.096	0
3b	0.156	0.195	0.66	0.028	0.046	-0.078	0.025	0.007	0.011	0.021	0.031	0.040	-
4	0.625	0.195	2.72	0.087	0.046	0.041	0.010	0.051	0.079	0.045	0.046	0.158	0.200
5	0.625	0.200	2.90	0.239	0.046	0.193	-0.112	0.081	0.027	0.052	0.077	0.460	0.600
5a	0.625	0.125	2.96	0.225	0.046	0.179	-0.135	0.044	0.015	0.031	0.010	0.410	-
5b	0.312	0.200	1.37	0.129	0.046	0.083	-0.052	0.031	0.023	0.019	0.014	0.210	0.300
5c	0.312	0.125	1.37	0.109	0.046	0.063	-0.046	0.015	0.011	0.016	0.012	0.130	-
6	0.625	0.200	2.94	0.23	0.046	0.184	-0.101	0.083	0.028	0.052	0.016	0.440	0.600
7	0.625	0.200	3.00	0.258	0.046	0.210	-0.095	0.115	-0.038	0.076	0.025	0.523	0.700
8	0.312	0.195	1.28	-0.029	0.046	-0.075	0.157	0.082	0.064	0.135	0.105	-0.30	-0.250

Figure 7.- Shapes, dimensions, and aerodynamic coefficients of the shrouds investigated. In the sketches, P = parallel to the axis. At the point of the shroud profile designated by ↓ is the location of the plane of rotation of the propeller.

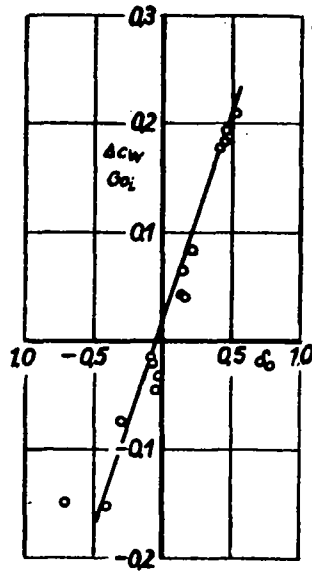


Figure 8.- The drag coefficient  $\Delta c_{W_{Go_i}}$  induced by the shroud on the nacelle by mutual influence as a function of the dimensionless mean additional velocity  $\delta_0 = \bar{v}_{R_S} / v$  (without propeller).

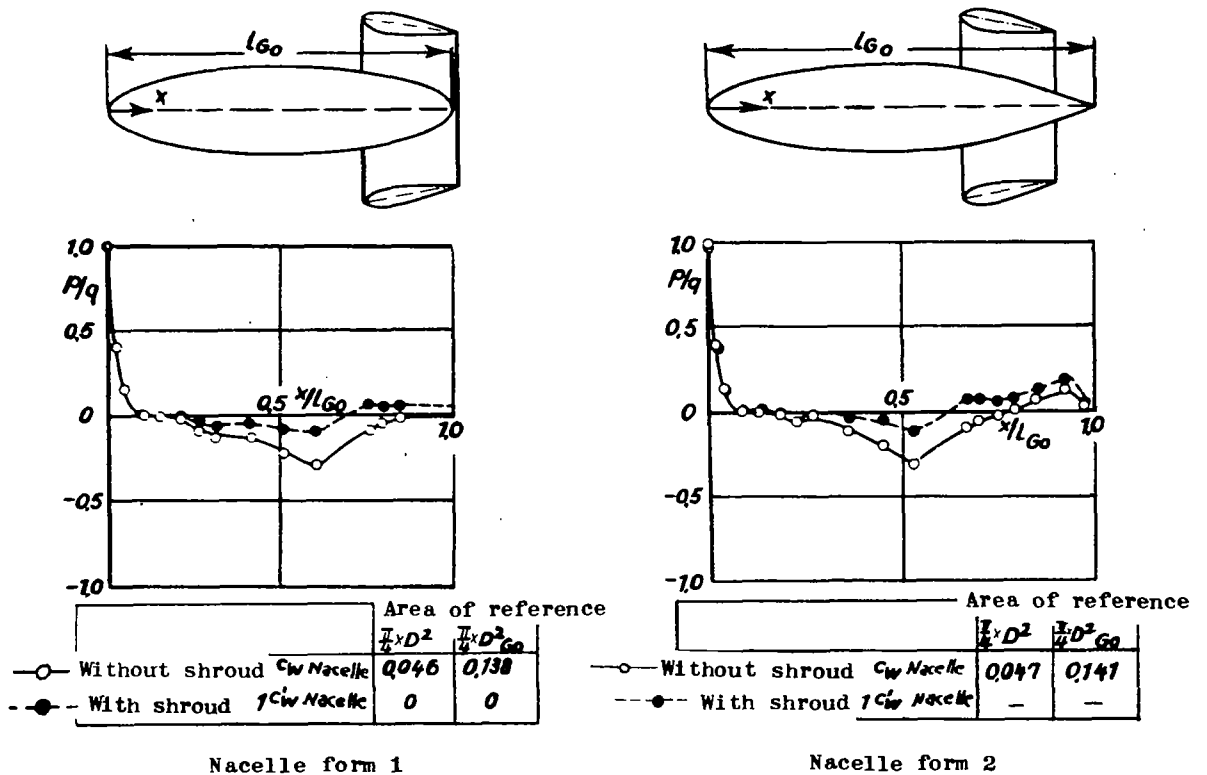


Figure 9.- Pressure distribution at the nacelle without and with shroud.

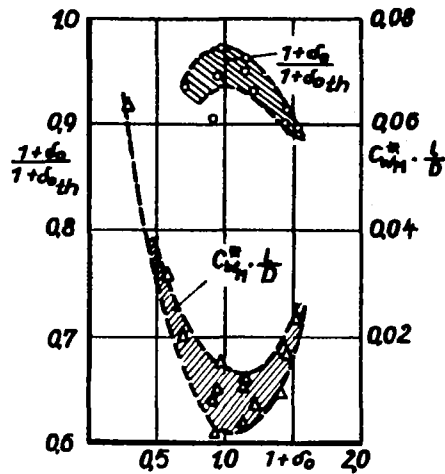


Figure 10.- Ratio of the measured  $(1 + \delta_0)$  and calculated  $(1 + \delta_{0th})$  mean axial flow velocity through the shroud (with nacelle, without propeller). Further, parasite shroud drag  $C_{wM}^* \cdot \frac{l}{D}$  as a function of the measured dimensionless mean flow velocity  $1 + \delta_0 = \bar{v}_{RS}/v$ .

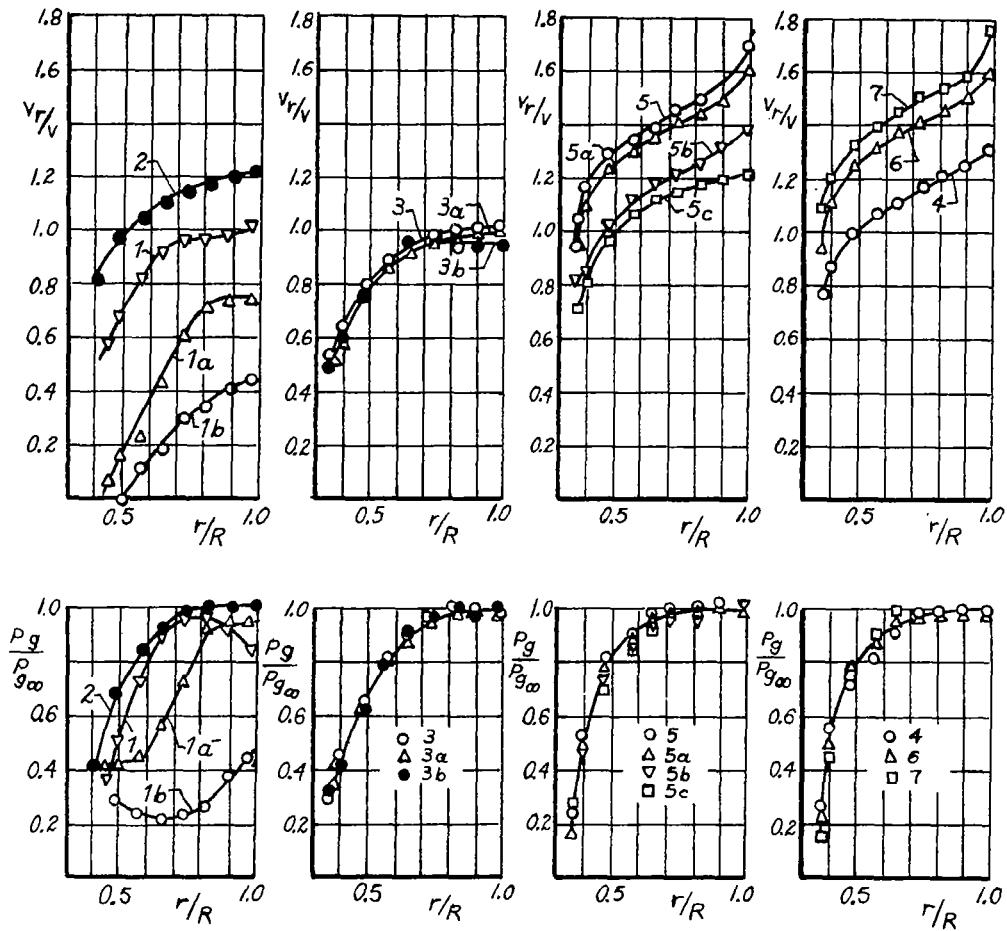


Figure 11.- Distribution of the axial flow velocity  $v_r$  and of the total pressure present shortly ahead of the blower plane  $p_g$  over the radius.  $R$  = outer radius of the propeller;  $v$  = free-stream velocity;  $p_{g_\infty}$  = total pressure in the undisturbed flow. The numbers designating the curves refer to the designation of the shroud according to figure 7.

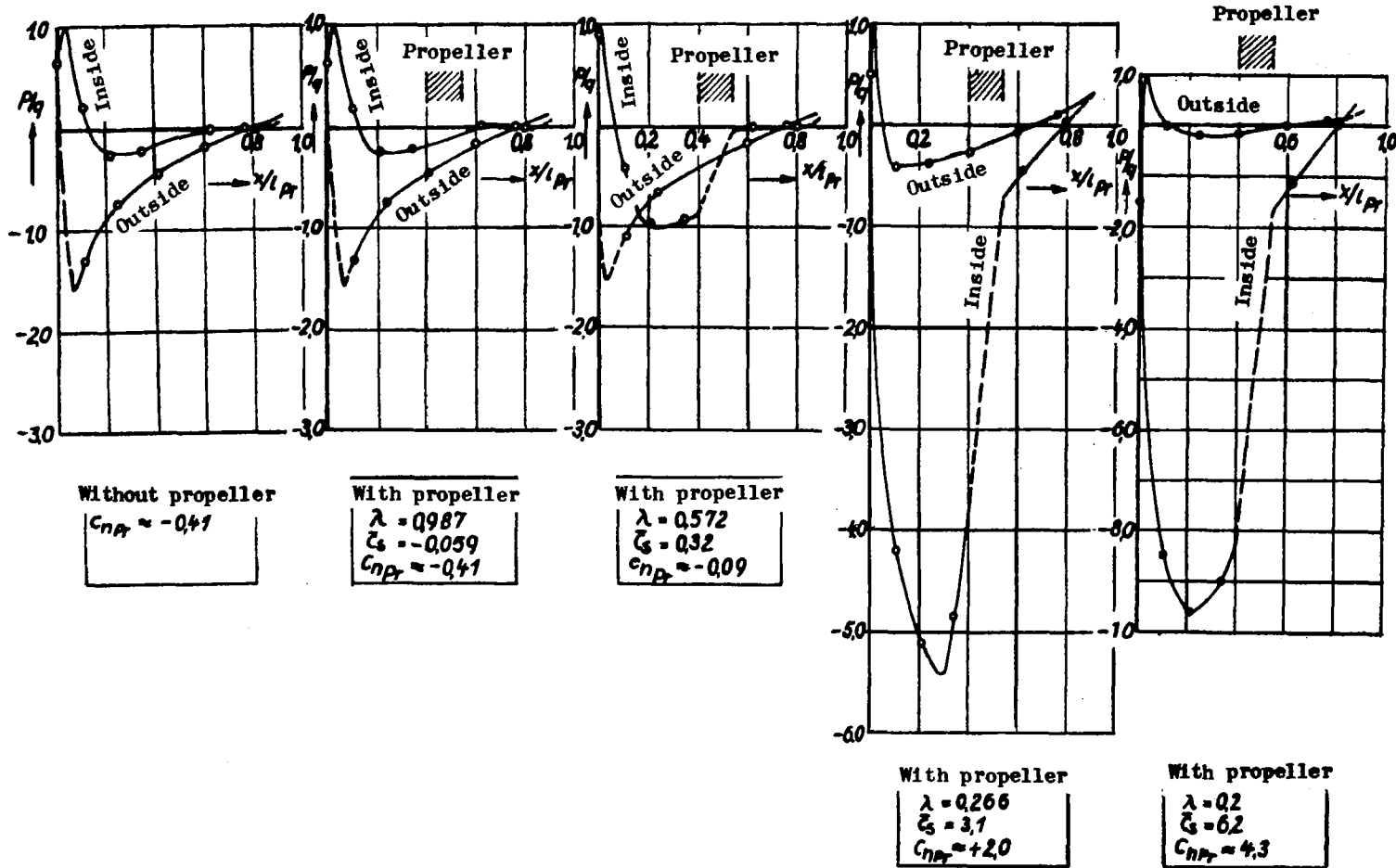


Figure 12.- Pressure distribution at the shroud profile 1 without propeller and with propeller 1 ( $\beta = 40^\circ$ ) for several ratios of advance  $\lambda$ .

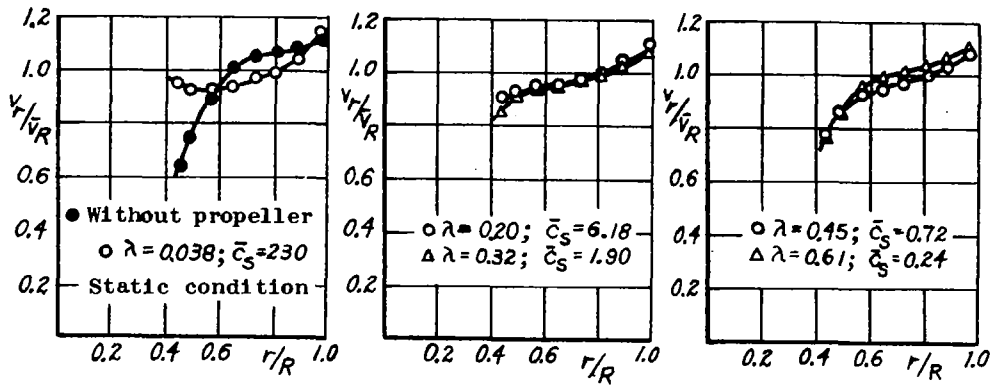


Figure 13.- Ratio of the velocity at the radius  $r$  and the mean axial flow velocity  $\bar{v}_R$  through the annular area immediately ahead of the plane of rotation of the propeller. Shroud 1 without propeller and with propeller 1 at  $\beta = 40^\circ$ .

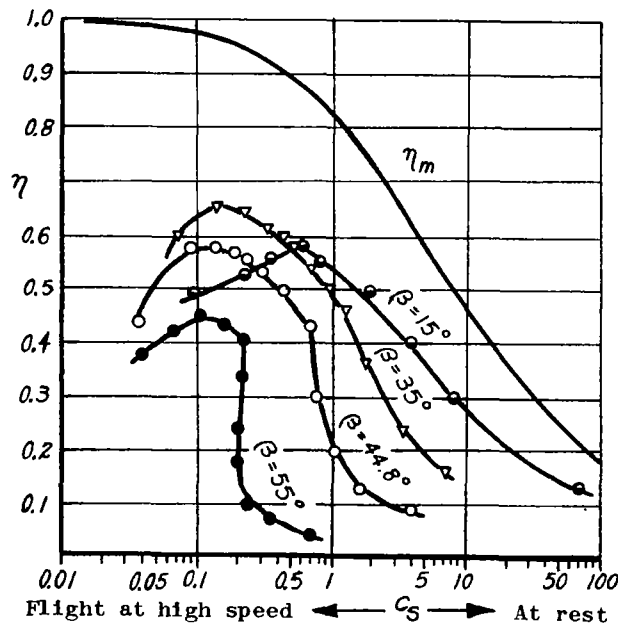


Figure 15.- Propeller 1 without shroud. Measured efficiency and maximum theoretical efficiency  $\eta_m = 2/(1 + \sqrt{1 + c_S})$  as a function of the measured loading  $c_S$ .

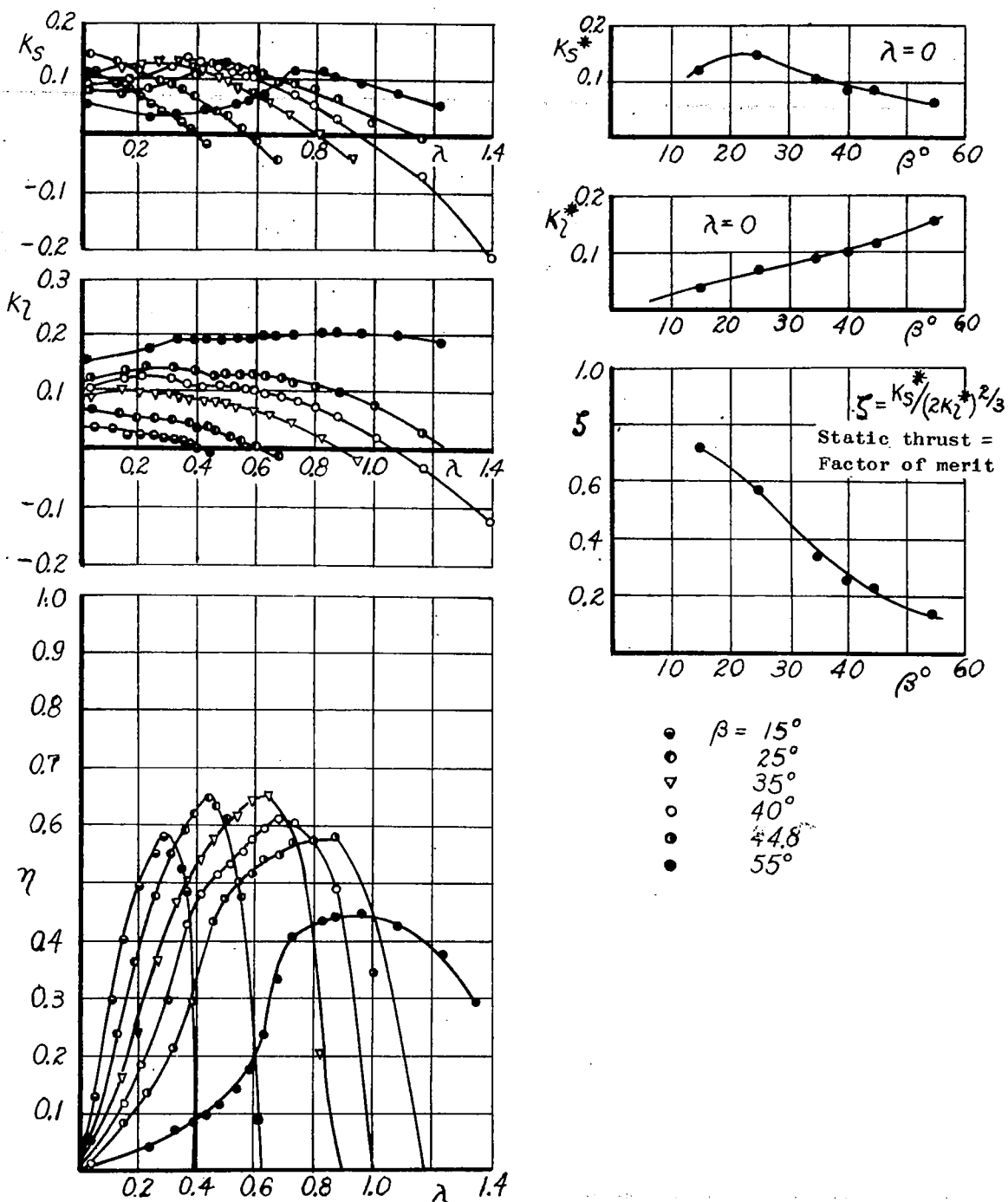


Figure 14.- Measured coefficients of the propeller without shroud 1 as functions of the ratio of advance and of the blade angle. Nacelle shape 1.

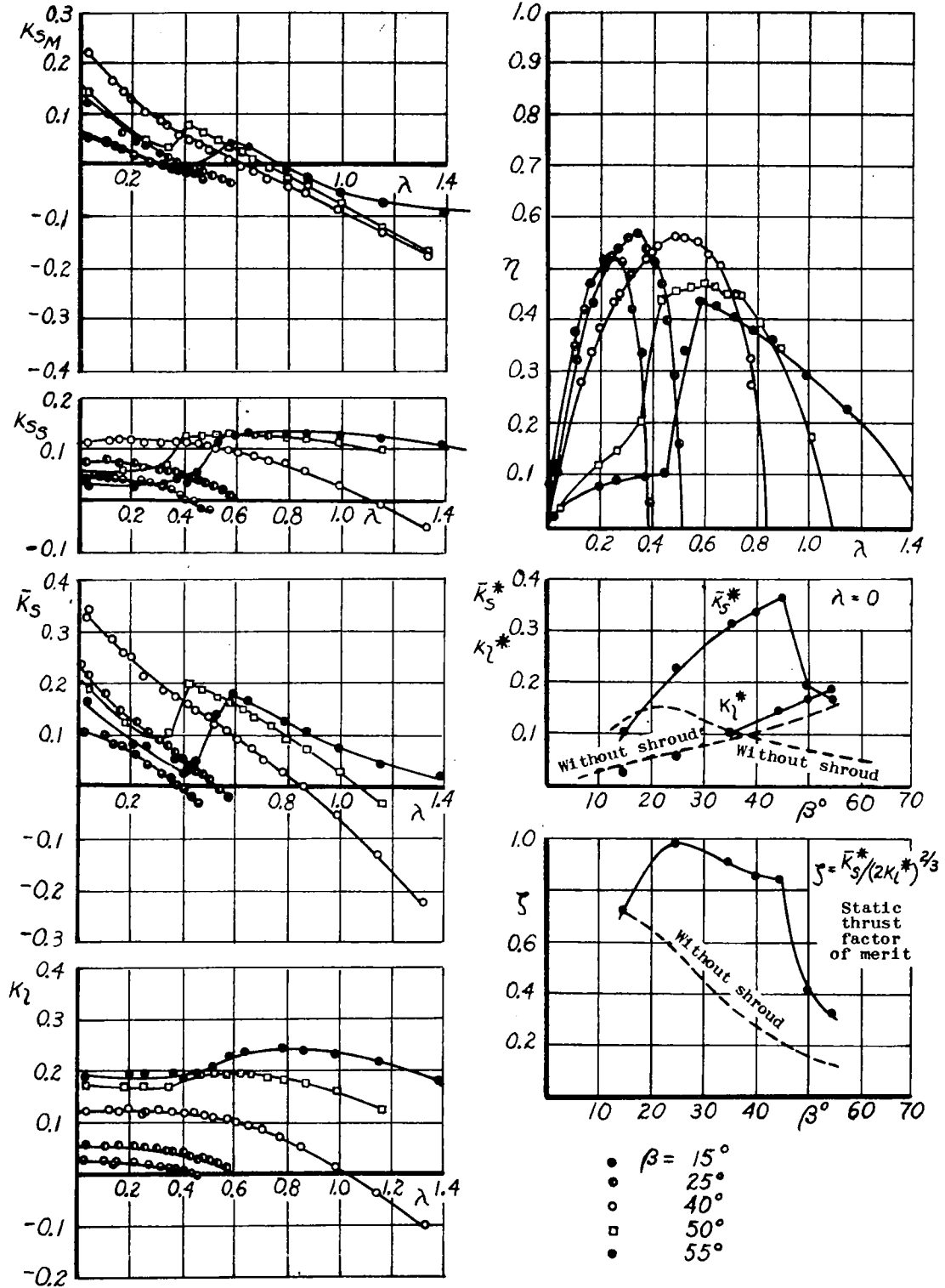


Figure 16.- Propeller 1 with shroud 1. Coefficients as functions of the ratio of advance and of the blade angle.

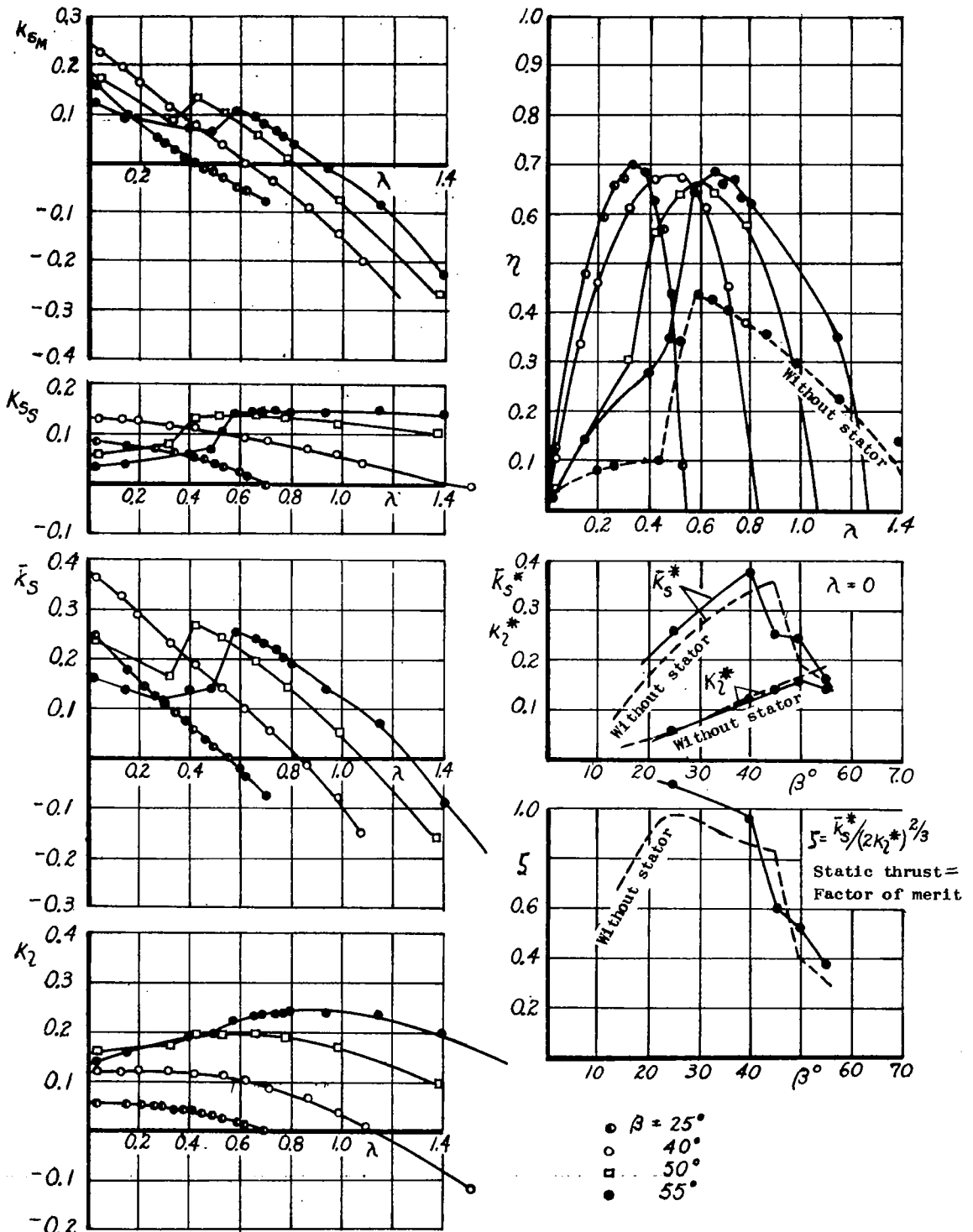


Figure 17.- Propeller 1 with exit stator and shroud 1. Coefficients as functions of the ratio of advance and of the blade angle. The partial thrust of the stator is contained in the coefficient of the shroud thrust  $k_{SM}$  because the stator was fixed to the shroud.

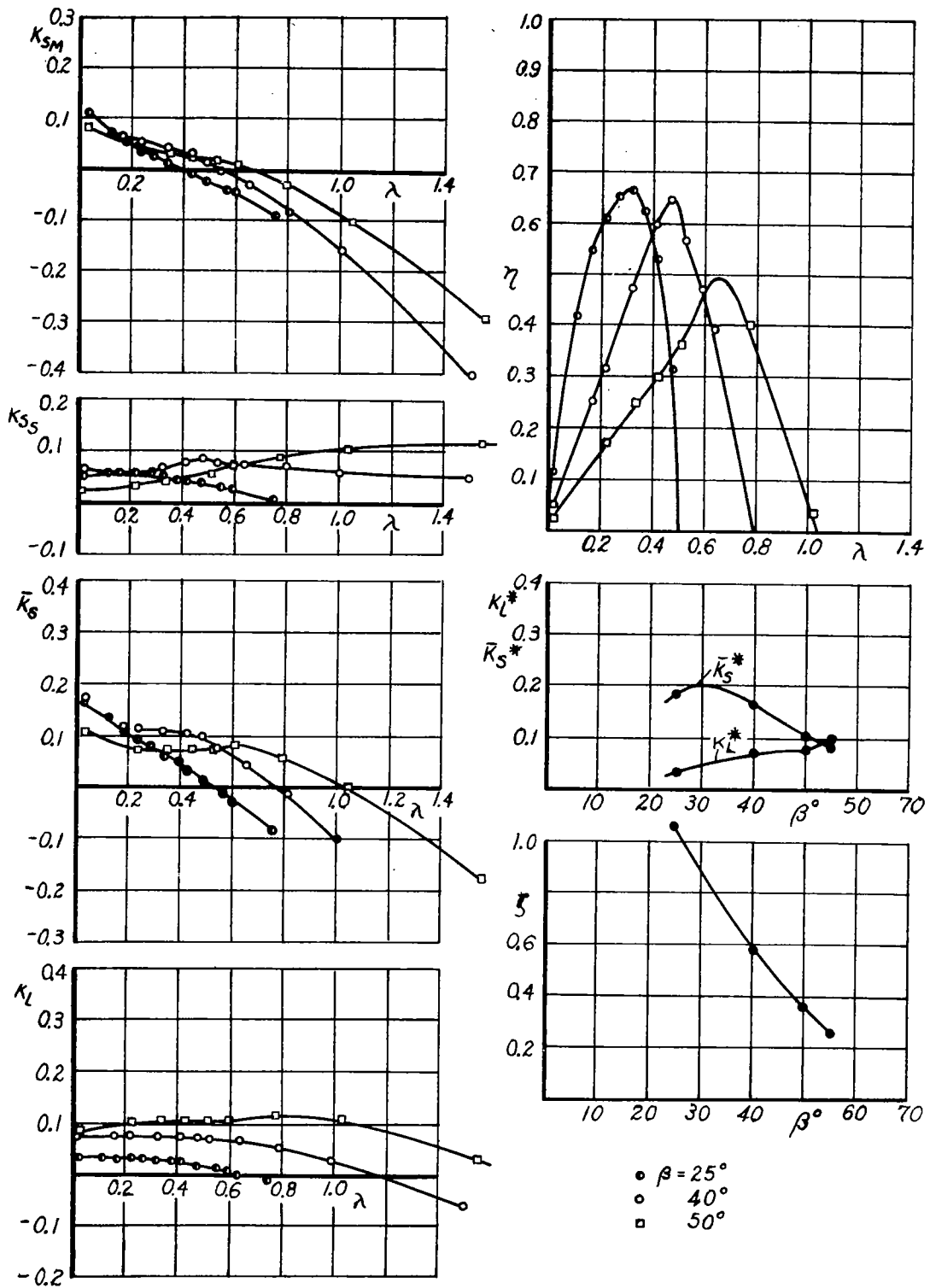


Figure 18.- Propeller 1, 4-bladed with exit stator and shroud 1. Coefficients as functions of the ratio of advance and of the blade angle. The partial thrust of the stator is contained in the value  $k_{SM}$ .

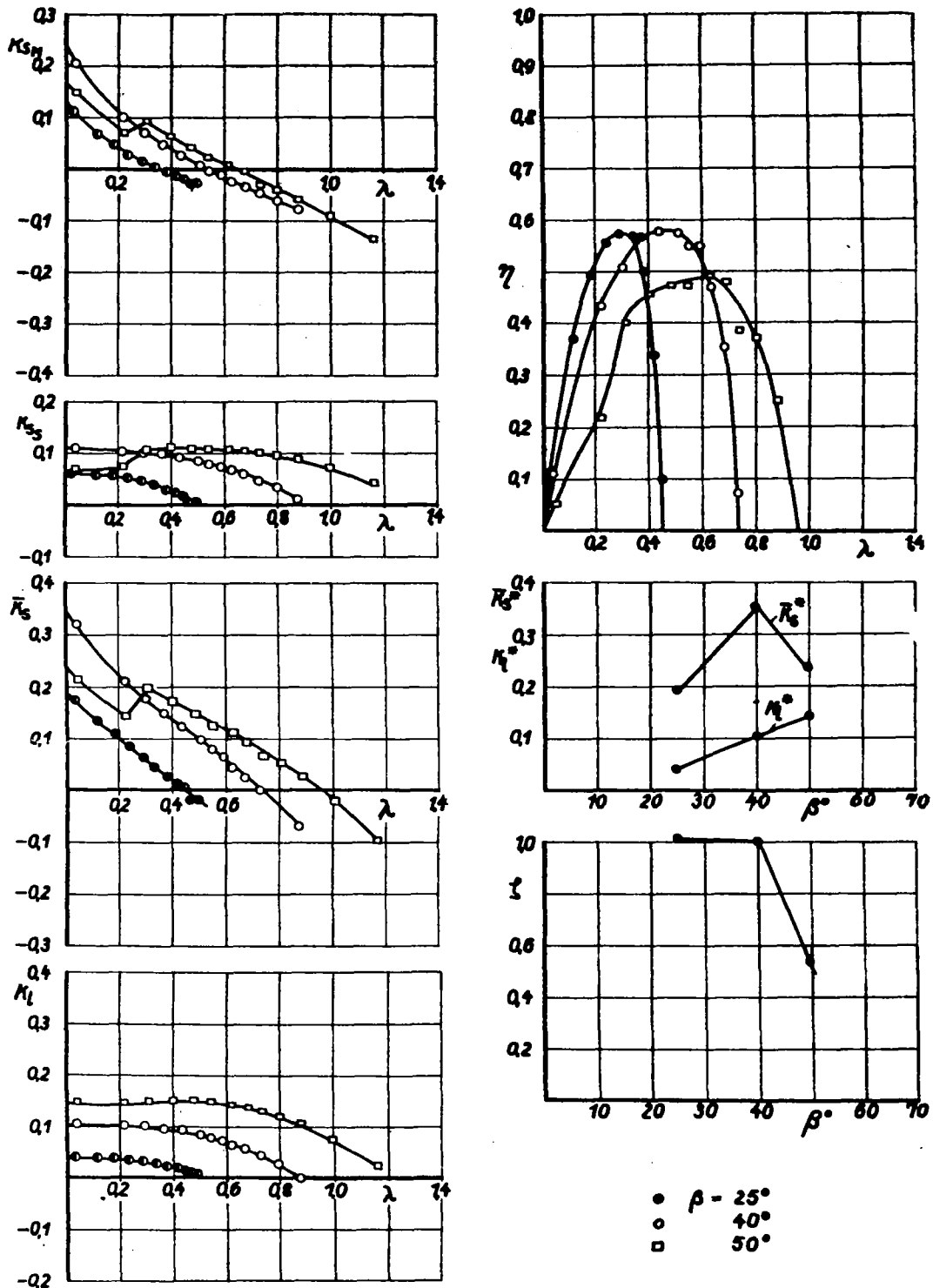


Figure 19.- Propeller 2 with shroud 1. Coefficients as functions of the ratio of advance and of the blade angle.

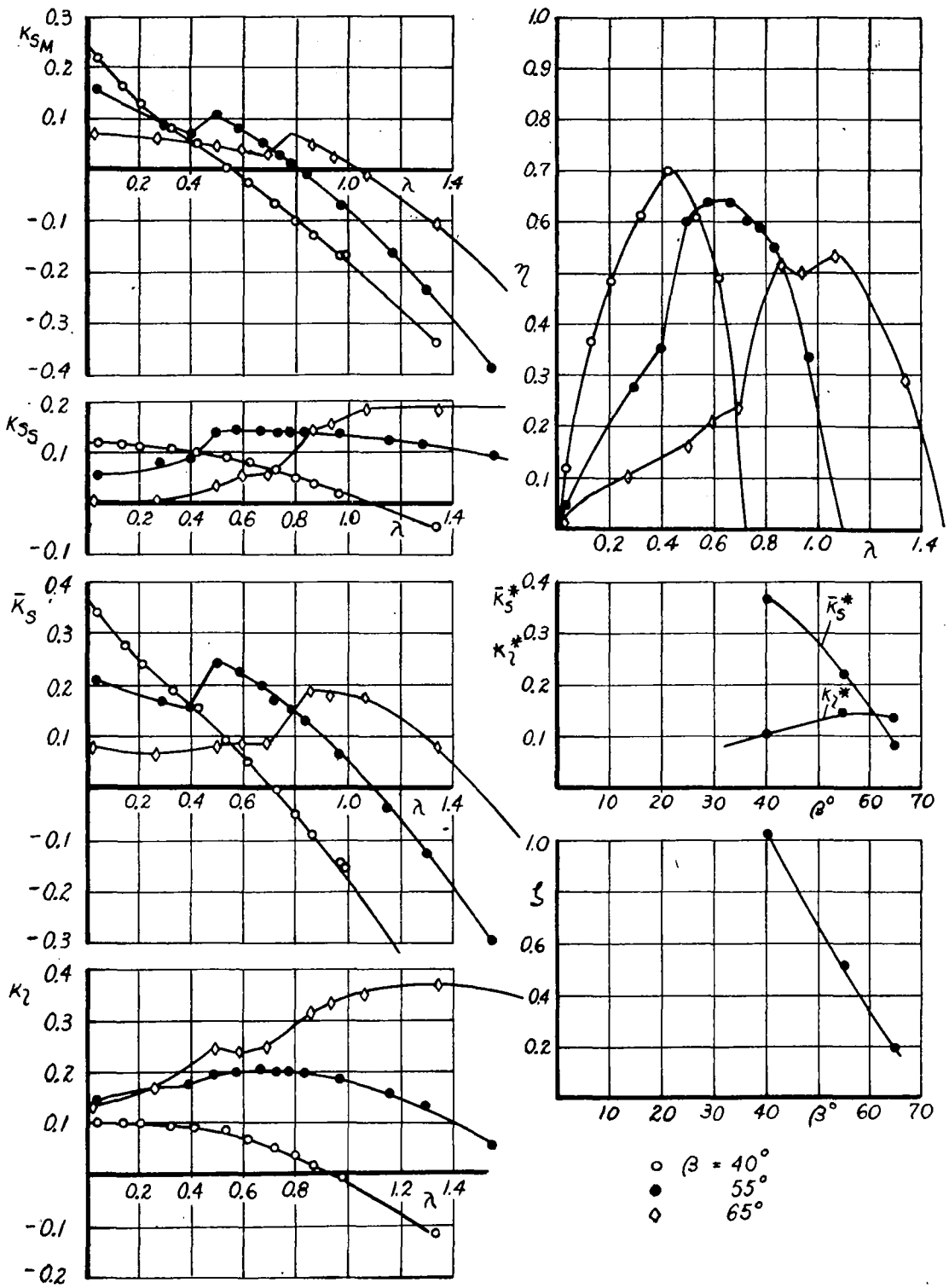


Figure 20.- Propeller 2 with exit stator and shroud 1. Coefficients as functions of the ratio of advance and of the blade angle. The partial thrust of the stator is contained in the value  $k_{SM}$ .

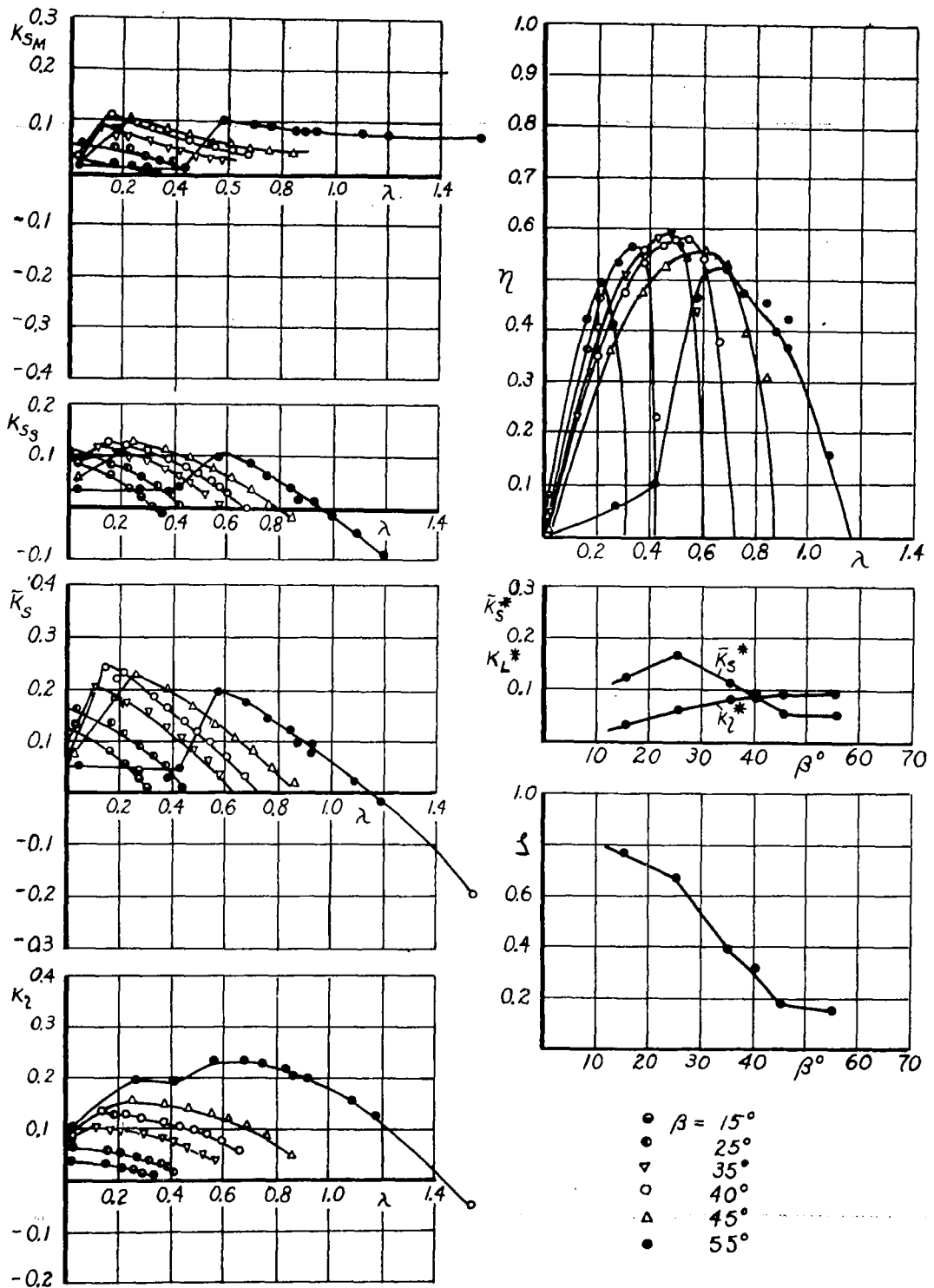


Figure 21.- Propeller 1 with shroud 5c. Coefficients as functions of the ratio of advance and of the blade angle.

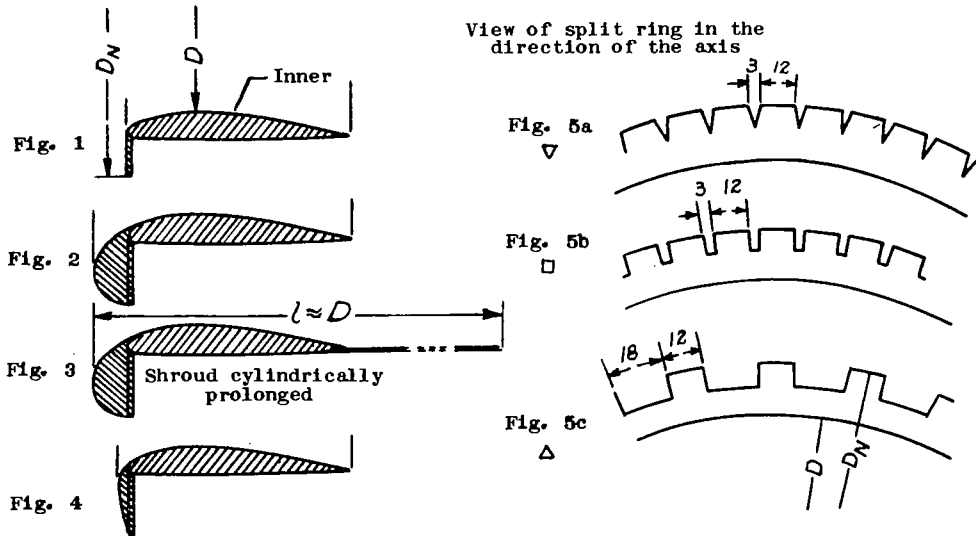
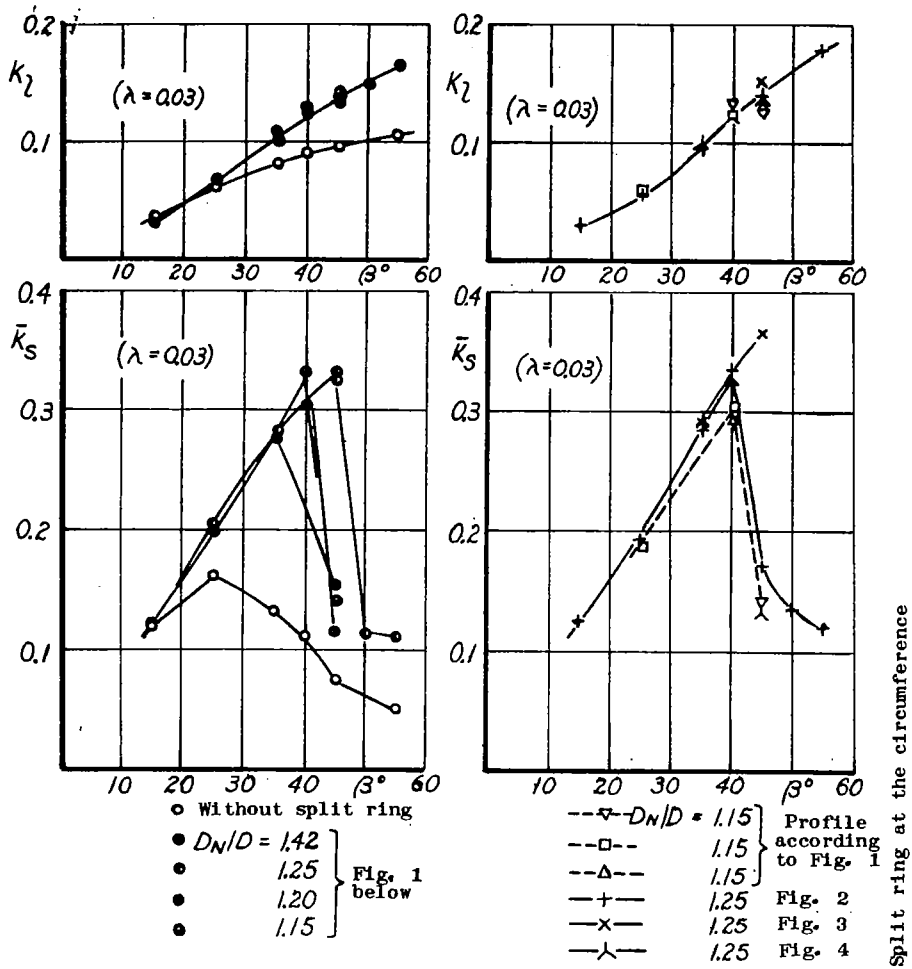


Figure 22.- Propeller 1 with shroud 5c. Improvement of the coefficients for static thrust conditions by use of a nose split ring.

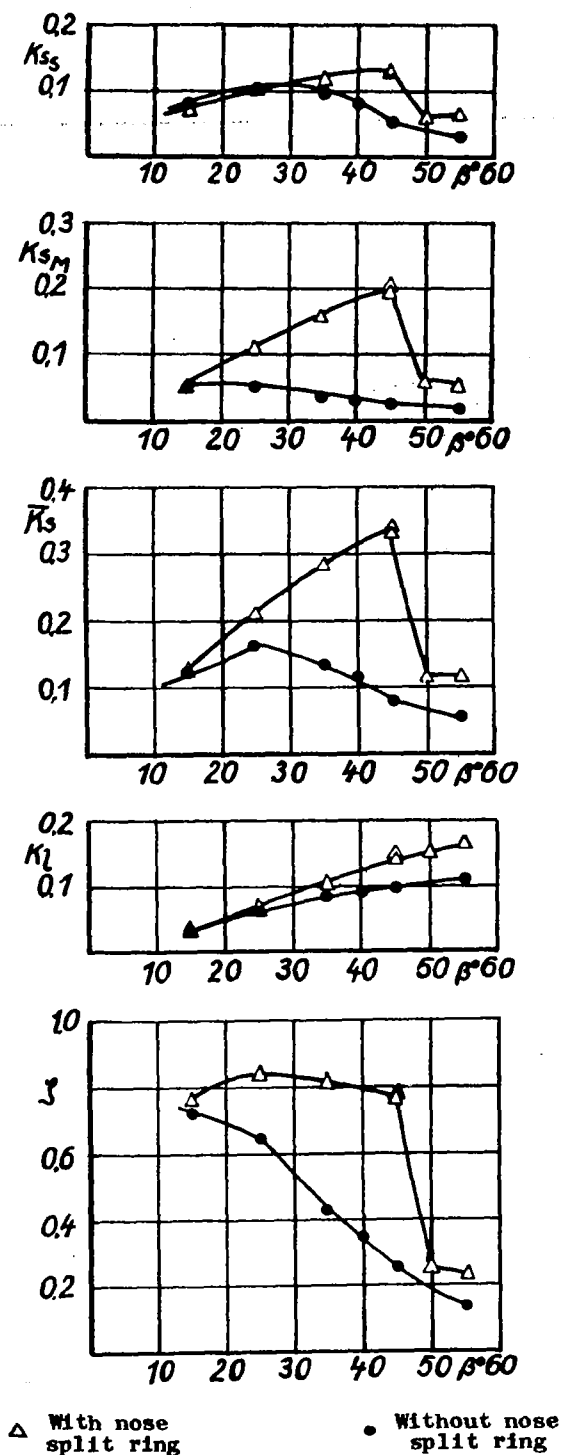
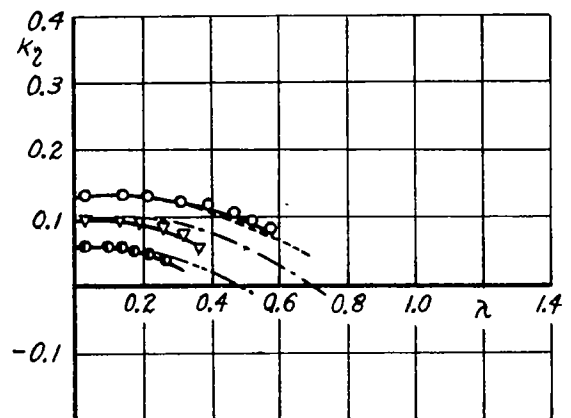
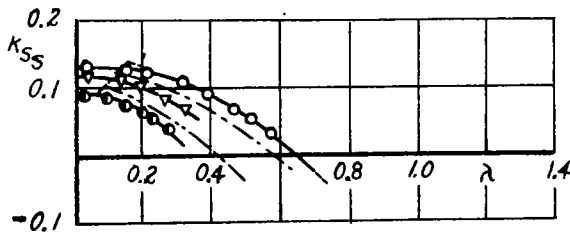
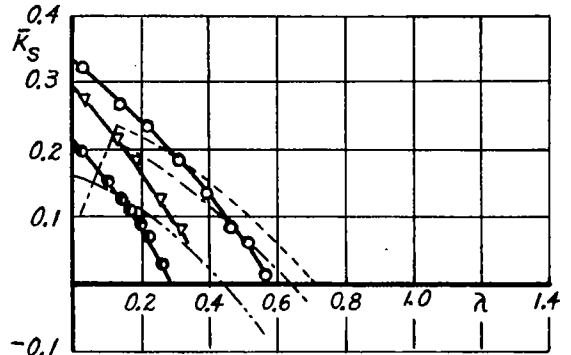
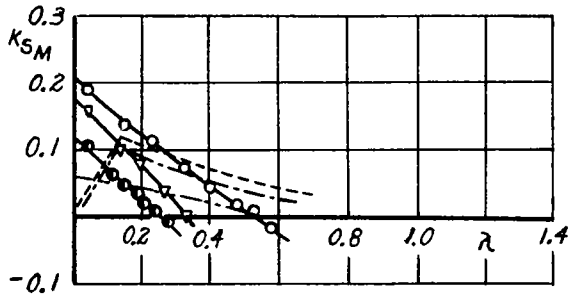
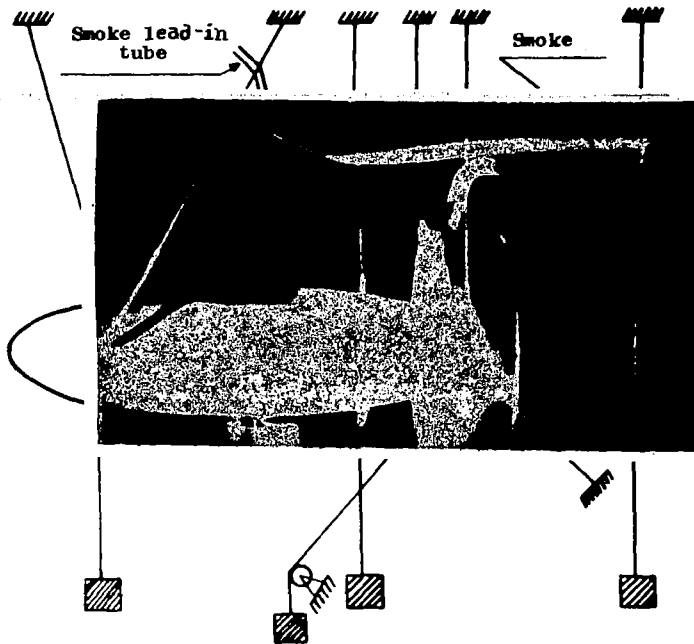


Figure 23.- Propeller 1 with shroud 5c. Improvement of the coefficients for static thrust conditions ( $\lambda \approx 0.03$ ) by use of a nose split ring.

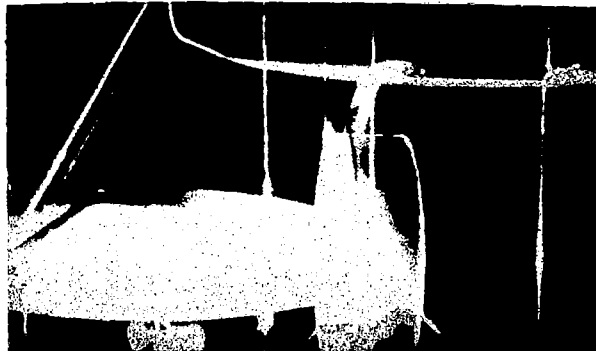


With nose split ring	○ $\beta = 40^\circ$
	▽ $35^\circ$
	● $25^\circ$
$\frac{D_N}{D} = 1.2$	
Without nose split ring	--- $\beta = 40^\circ$
	--- $35^\circ$
	--- $25^\circ$

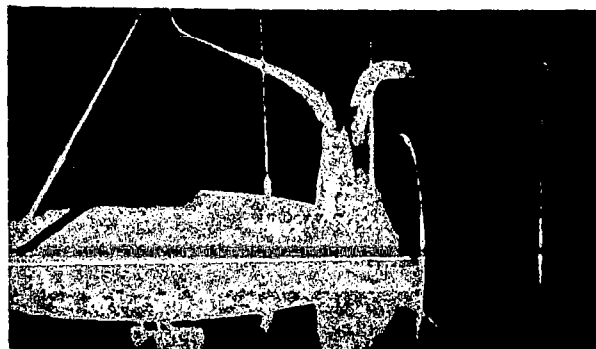
Figure 24.- Propeller 1 with shroud 5c. Coefficients as functions of the ratio of advance and of the blade angle for the cases "without" and "with nose split ring".



a. Free wheel



b.  $\lambda = 0.21$   
 $\bar{c}_s = 3.6$



c.  $\lambda = 0.07$   
 $\bar{c}_s = 51.0$

Figure 25a-c.- Flow at shroud 5c with nose split ring made visible by smoke method. Propeller 1,  $\beta = 35^\circ$ , without exit stator.



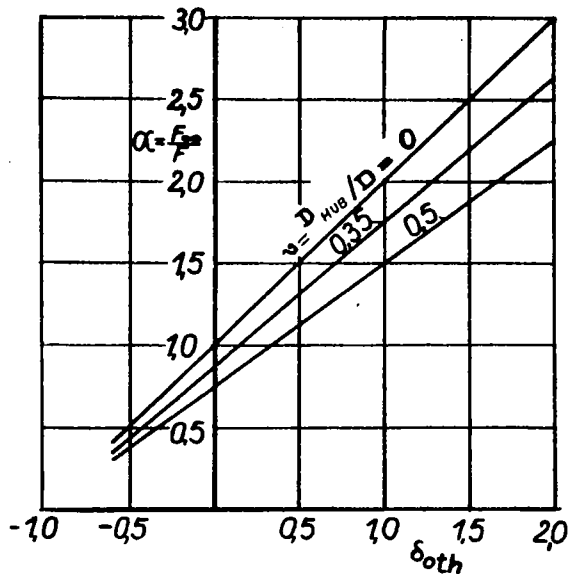


Figure 26.- Dependence of the slipstream cross section ratio on the theoretical nondimensional additional velocity  $\delta_{0th}$  and on the hub ratio (according to equation (7)).

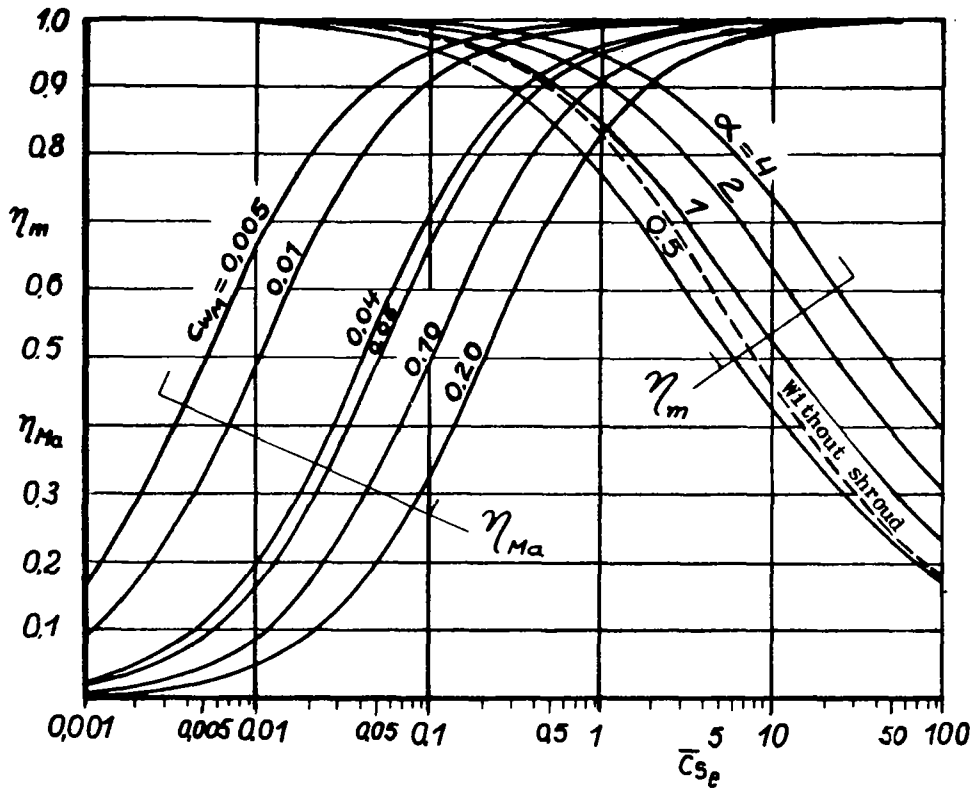


Figure 27.- Maximum theoretical efficiency  $\eta_m$  according to equation (10) and shroud efficiency  $\eta_{Ma}$  according to equation (14) as functions of the effective total thrust loading  $\bar{c}_{s_e}$ . The dashed-line curve applies to the propeller without shroud  $\eta_m = 2/(1 + \sqrt{1 + c_s})$ .  $c_{wM}$  is the parasite drag coefficient of the shroud, referred to  $D^2\pi/4$ .

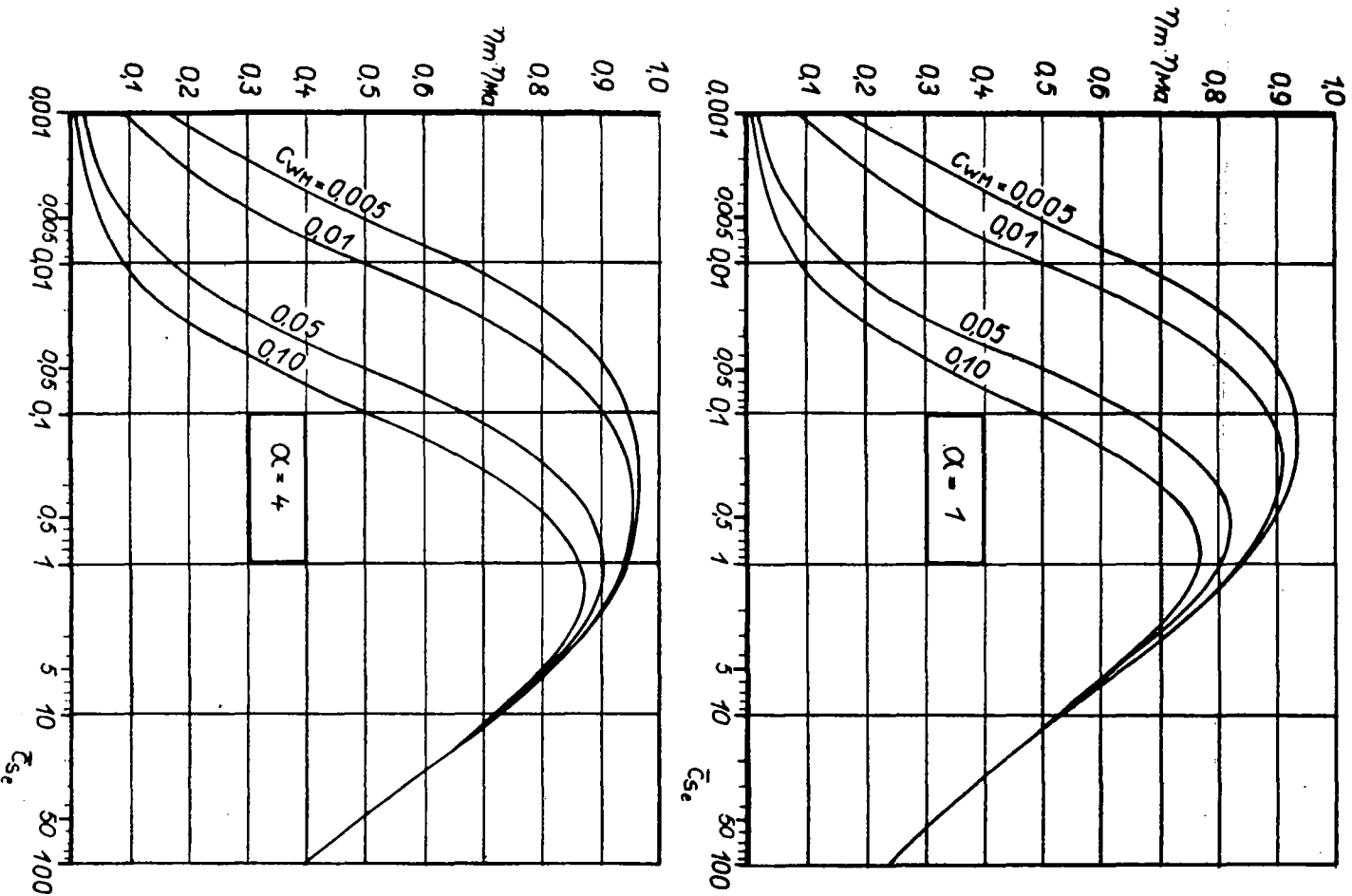


Figure 28. - Product of the maximum theoretical efficiency and of the shroud efficiency as a function of the effective total thrust loading for various slipstream cross section ratios  $\alpha$  and shroud drags  $C_w M$ .

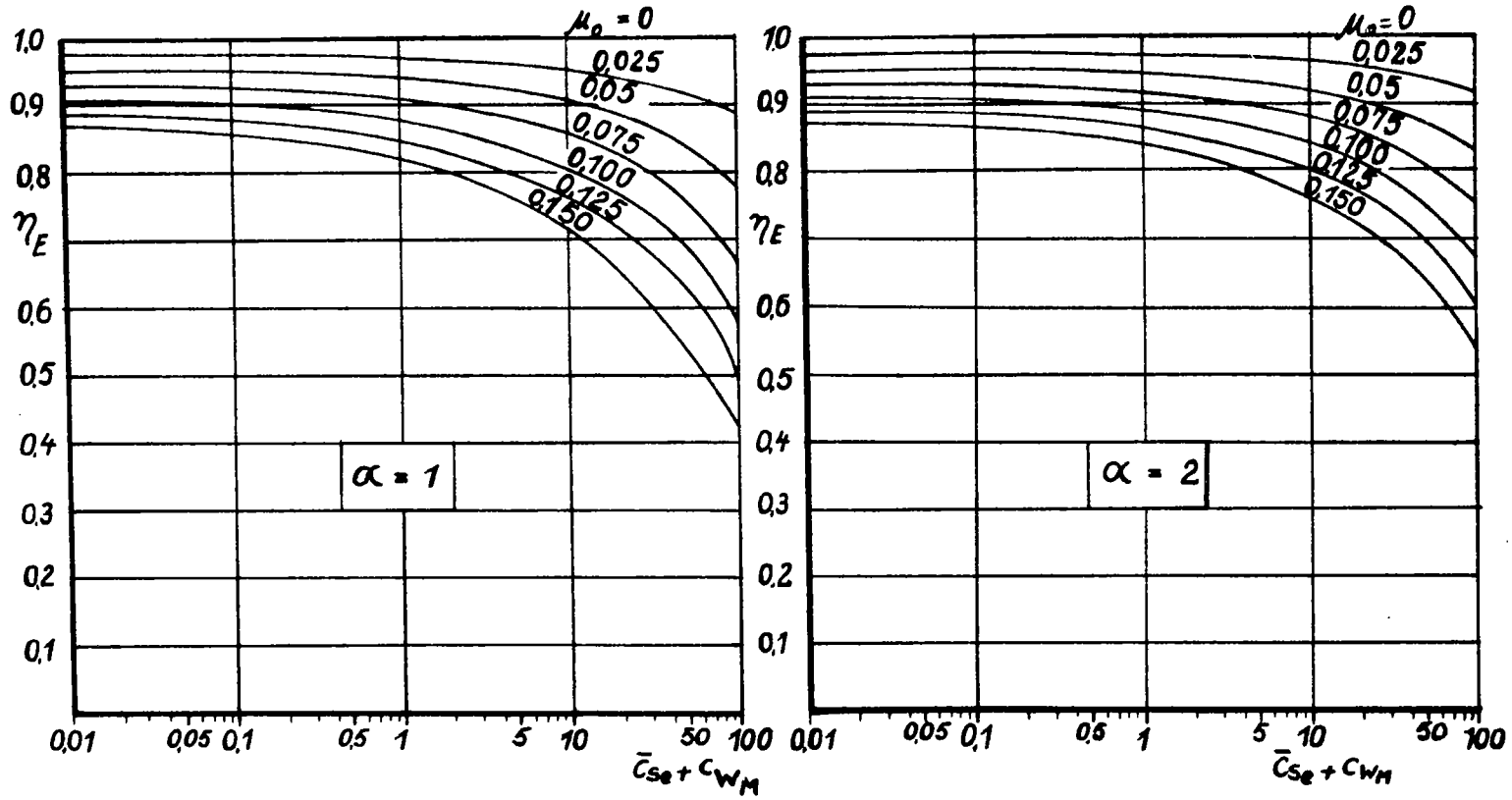


Figure 29.- Dependence of the installation efficiency  $\eta_E$  on  $\bar{c}_{se} + c_{wm}$ . Parameter: slipstream cross section ratio and pressure loss coefficient  $\mu_0$ .

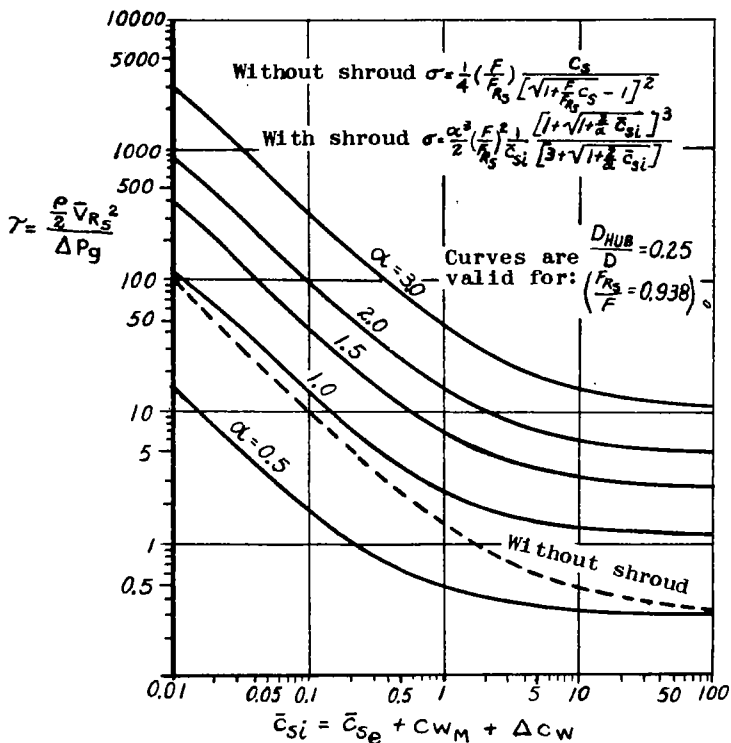


Figure 30a.- Variation of the operating condition of the blower

$\sigma = \frac{\rho}{2} \frac{\bar{v}_{R_s}^2}{\Delta p_g}$  with the induced loading  $\bar{c}_{s_e} + c_{w_M} + \Delta c_w$  for various slipstream cross section ratios  $\alpha$ , i.e., various shroud shapes.

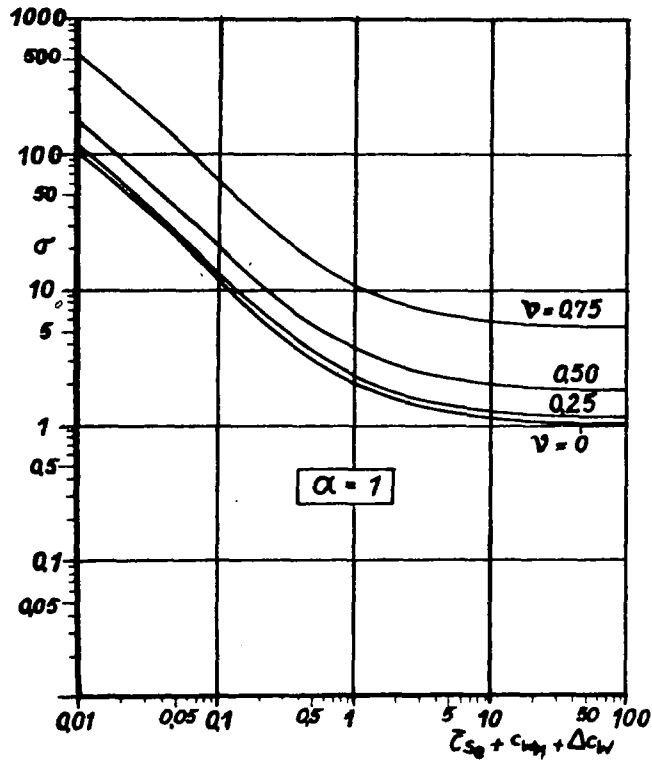


Figure 30b.- Dependence of the operating condition of the blower

$\sigma = \frac{\rho \bar{v}}{2} R_S^2 / \Delta p_g$  on the induced loading  $\bar{c}_{s_e} + c_{w_M} + \Delta c_w$  for a shroud which yields the slipstream cross section ratio  $\alpha = 1$ . Parameter: hub ratio  $v = D_{\text{hub}}/D$ .

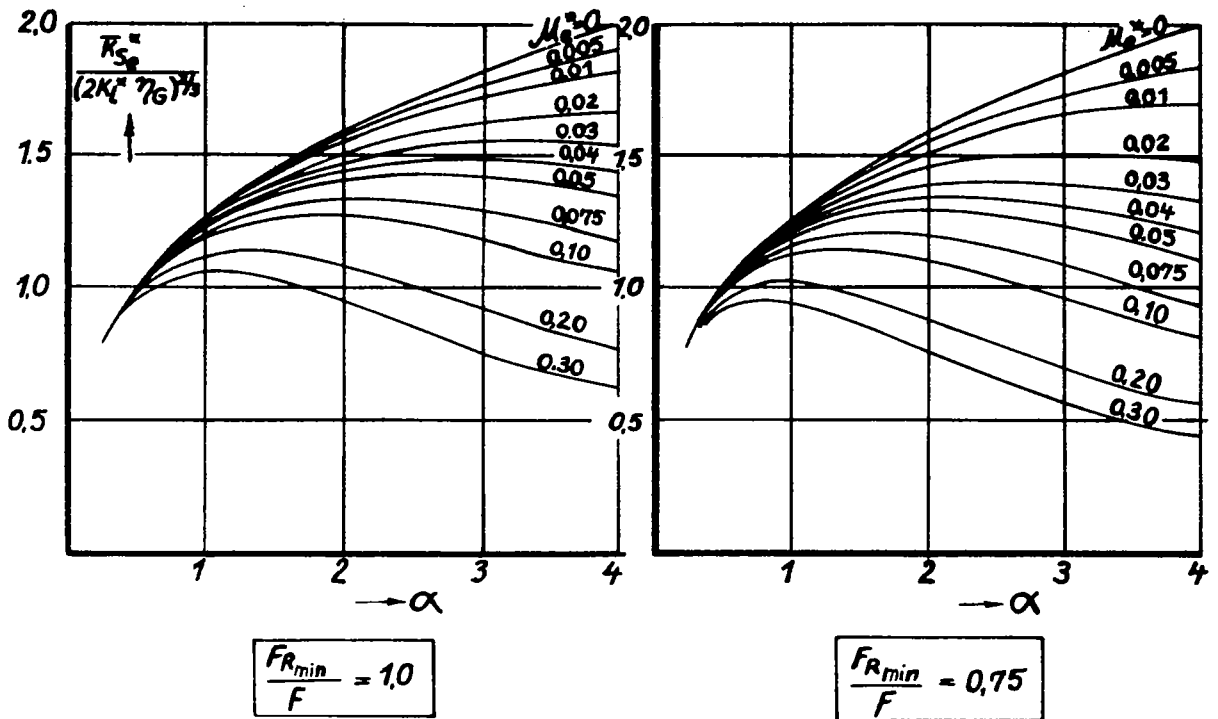


Figure 31.- Influence of the slipstream cross section ratio  $\alpha$ , the pressure loss coefficient  $p_{e^*} \times \Delta p_{v^*} / \frac{\rho}{2} \bar{v}_{R_S}^2$  and the hub ratio  $u = D_{hub} / D$  on the static thrust behavior of shrouded propellers.

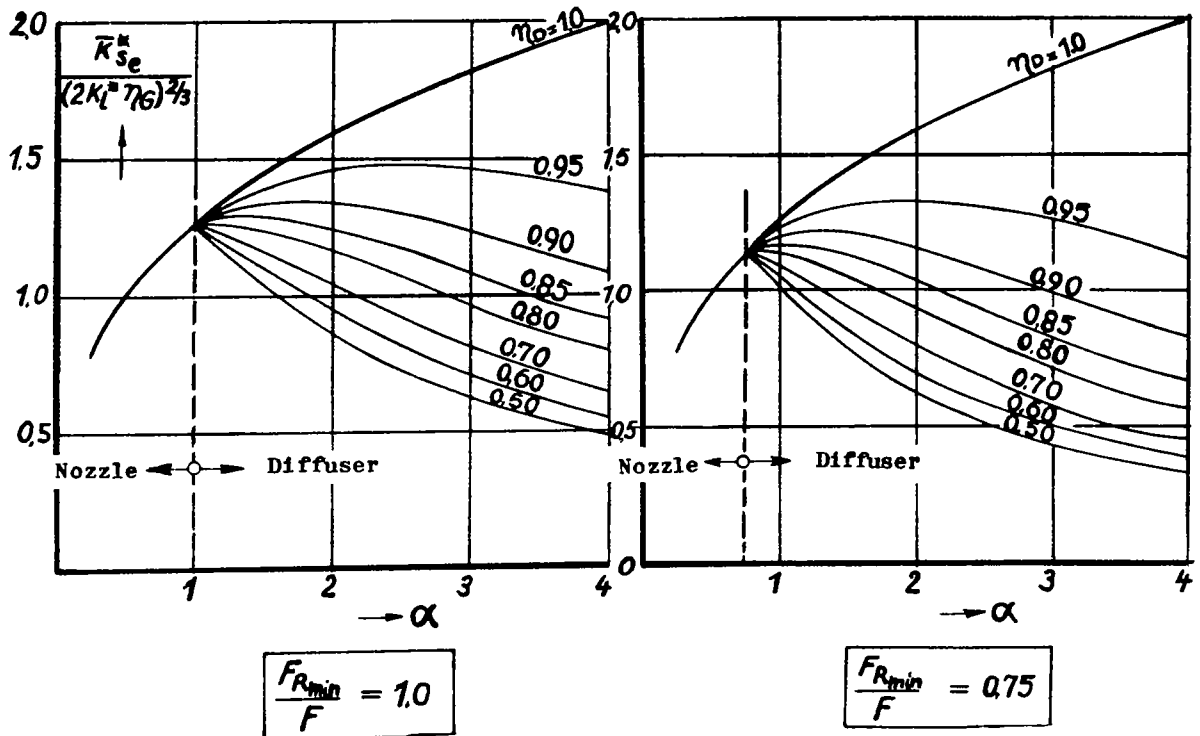
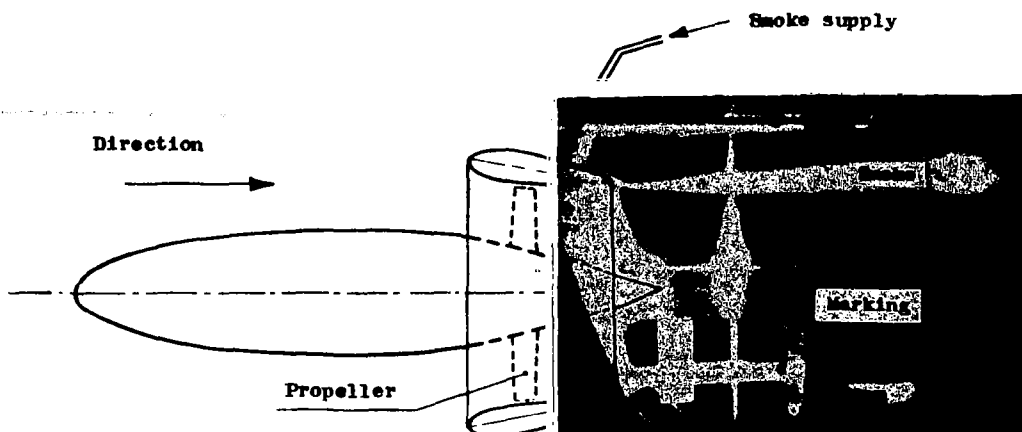
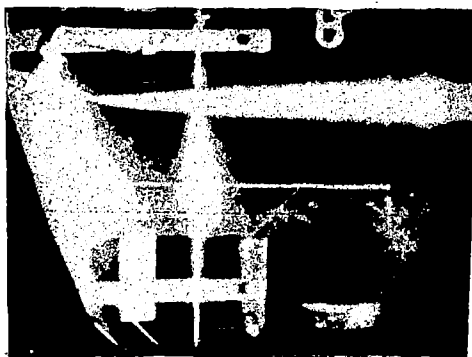


Figure 32.- Influence of the slipstream cross section ratio  $\alpha$ , the diffuser efficiency  $\eta_D$ , and the hub ratio  $v$  on the static thrust behavior.



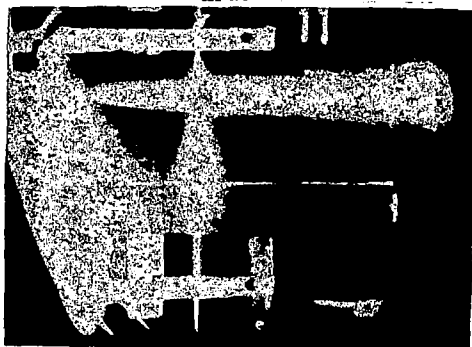
Propeller 2,  $\beta = 40^\circ$ , with stator,  
 $\lambda = 0,07$ ,  $\bar{c}_s = 66,0$



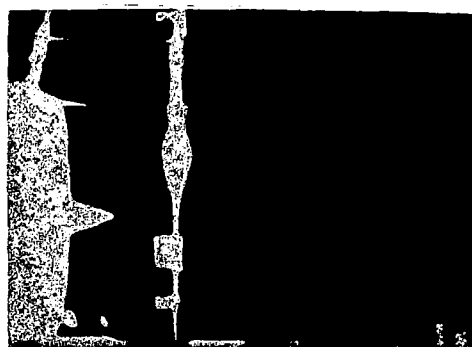
Propeller 2,  $\beta = 40^\circ$ , with stator,  
 $\lambda = 0,40$ ,  $\bar{c}_s = 0,98$



Propeller 2,  $\beta = 40^\circ$ , with stator,  
 $\lambda = 0,80$ ,  $\bar{c}_s = -0,07$



Propeller 2,  $\beta = 40^\circ$ , with stator,  
 $\lambda = 1,0$ ,  $\bar{c}_s = -0,17$



Without propeller and  
 without stator

Figure 33.- Jet boundaries behind the shroud made visible by smoke test. Shroud 1 with propeller 2 ( $\beta = 40^\circ$  with exit stator). Below, right: shroud 1 without propeller.



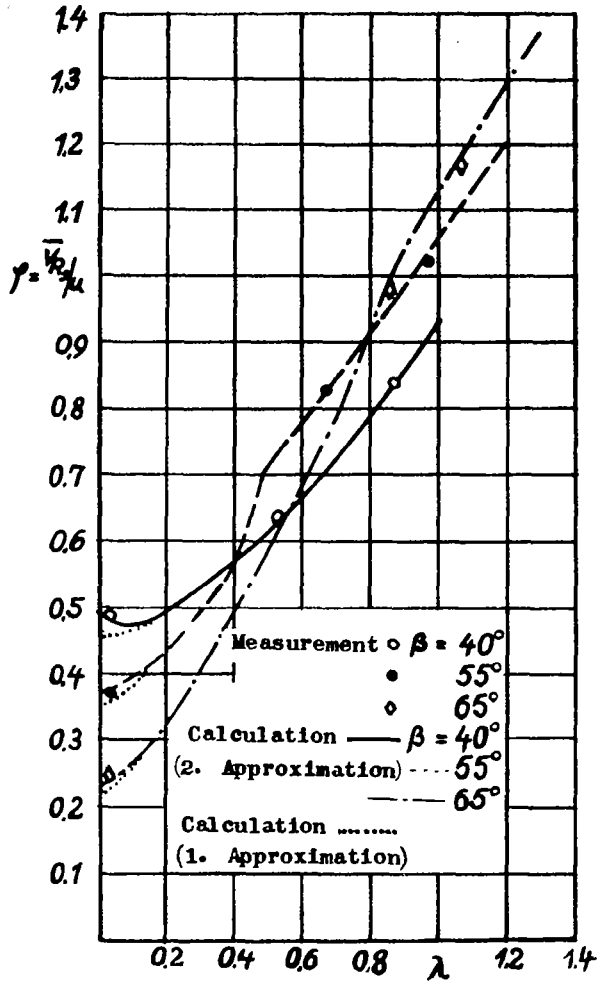


Figure 34.- Comparison between calculation and measurement with respect to the dependence of the mass coefficient  $\phi = v_{RS}/u = (1 + \delta_g) \lambda$  on the ratio of advance. Valid for propeller 2 with exit stator and shroud 1.

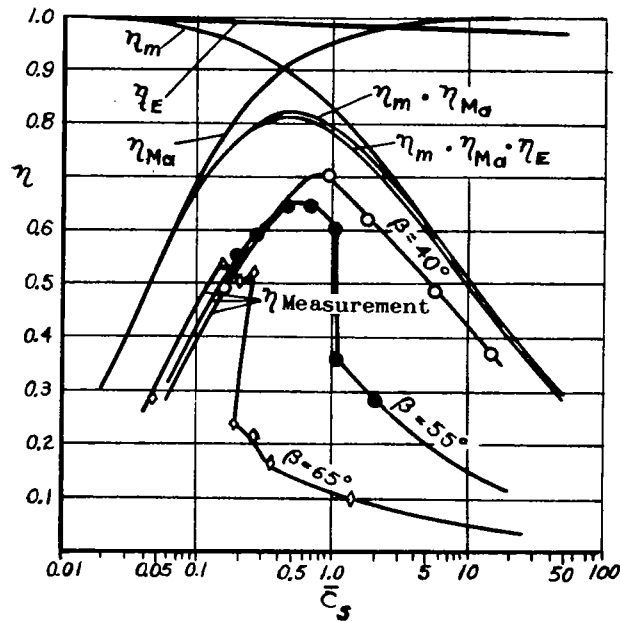


Figure 35.- Measured efficiencies and calculated partial efficiencies as functions of the total thrust loading ratio. Valid for propeller 2 with exit stator and shroud 1.

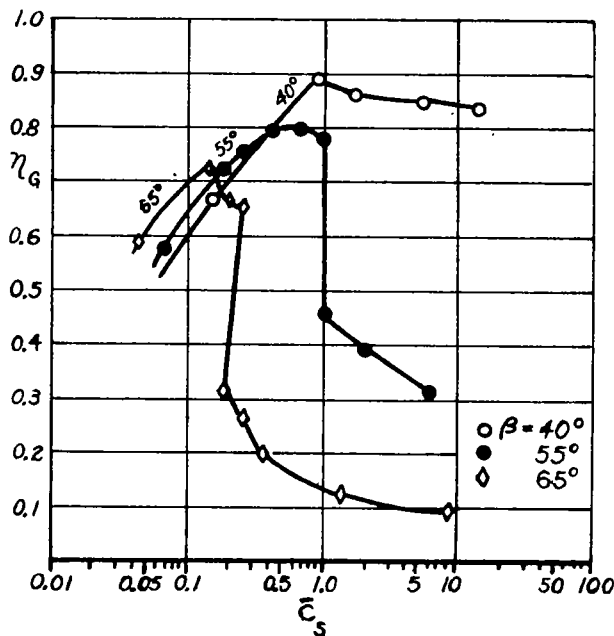
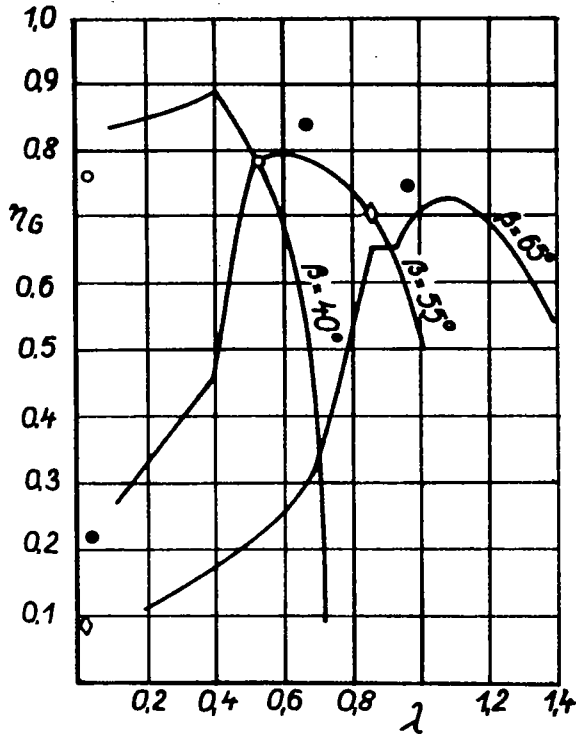


Figure 36.- Propeller 2 with exit stator and shroud 1. The blower efficiency probable according to calculation  $\eta_G = \eta_{\text{measured}} / (\eta_m \times \eta_{Ma} \times \eta_E)_{\text{calculated}}$  as function of the total thrust loading ratio.



Curves drawn in:  $\eta_6 = \frac{\eta_{\text{measured}}}{(\eta_m \cdot \eta_{M2} \cdot \eta_E)}$  calculation

$\circ$   $\beta = 40^\circ$   
 $\bullet$   $55^\circ$   
 $\diamond$   $65^\circ$ 
} From measurement

Figure 37.- Comparison between the blower efficiency probable according to calculation and the actually existing blower efficiency. Propeller 2 with exit stator and shroud 1.